Probabilistic Engineering Mechanics 38 (2014) 22–34

Contents lists available at ScienceDirect

Probabilistic Engineering Mechanics

journal homepage: www.elsevier.com/locate/probengmech

A hybrid polynomial dimensional decomposition for uncertainty quantification of high-dimensional complex systems ☆

Vaibhav Yadav *, Sharif Rahman

College of Engineering, The University of Iowa, Iowa City, IA 52242, USA

ARTICLE INFO

Article history:
Received 3 December 2013
Received in revised form
3 July 2014
Accepted 5 August 2014
Available online 15 August 2014

Keywords:
ANOVA
HDMR
Dimension reduction
Stochastic dynamics

ABSTRACT

This paper presents a novel hybrid polynomial dimensional decomposition (PDD) method for stochastic computing in high-dimensional complex systems. When a stochastic response does not possess a strongly additive or a strongly multiplicative structure alone, then the existing additive and multiplicative PDD methods may not provide a sufficiently accurate probabilistic solution of such a system. To circumvent this problem, a new hybrid PDD method was developed that is based on a linear combination of an additive and a multiplicative PDD approximation, a broad range of orthonormal polynomial bases for Fourier-polynomial expansions of component functions, and a dimension-reduction or sampling technique for estimating the expansion coefficients. Two numerical problems involving mathematical functions or uncertain dynamic systems were solved to study how and when a hybrid PDD is more accurate and efficient than the additive or the multiplicative PDD. The results show that the univariate hybrid PDD method is slightly more expensive than the univariate additive or multiplicative PDD approximations, but it yields significantly more accurate stochastic solutions than the latter two methods. Therefore, the univariate truncation of the hybrid PDD is ideally suited to solving stochastic problems that may otherwise mandate expensive bivariate or higher-variate additive or multiplicative PDD approximations. Finally, a coupled acoustic-structural analysis of a pickup truck subjected to 46 random variables was performed, demonstrating the ability of the new method to solve large-scale engineering problems.

1. Introduction

Polynomial dimensional decomposition (PDD) is a hierarchical and convergent expansion of a general, high-dimensional stochastic response function in terms of polynomial functions of input variables with increasing dimensions [1–4]. The decomposition ameliorates the curse of dimensionality [5] to some extent by developing an input–output behavior of complex systems with low effective dimensions [6], wherein the degrees of interactions between input variables attenuate rapidly or vanish altogether. However, the original PDD, referred to as the additive PDD (A-PDD) in this paper, constitutes a sum of lower-dimensional component functions and is, therefore, predicated on an additive nature of a multivariate function decomposition. In contrast, when a response function is of a multiplicative nature, suitable multiplicative-type decompositions, such as the factorized PDD (F-PDD) [7], should be explored. Nonetheless, A-PDD or F-PDD is relevant as long as the dimensional hierarchy of a stochastic response is also additive or multiplicative. Unfortunately, the dimensional structure of a response function, in general, is not known a priori. Therefore, indiscriminately using A-PDD or F-PDD for general stochastic analysis is not desirable. Further complications may arise when a complex system exhibits a response that is dominantly neither additive nor multiplicative. In the latter case, hybrid approaches coupling both additive and multiplicative decompositions, preferably selected optimally, are needed. For such decompositions, it is unknown which truncation parameter should be selected when compared with that for A-PDD or F-PDD. More specifically, is it possible for the univariate truncation of a hybrid decomposition to produce stochastic solutions that are as good as or close to those obtained from higher-variate truncations of A-PDD or F-PDD? If the answer is yes, then a significant cost saving for high-dimensional uncertainty quantification is anticipated. That is the principal motivation of this work.

This paper presents a new hybrid PDD method for solving general high-dimensional stochastic problems commonly encountered in engineering and applied sciences. Section 2 provides a brief exposition of the existing additive and multiplicative PDD approximations, setting the stage for the new method developed. The hybrid PDD method, optimally blending A-PDD and F-PDD approximations, is described in Section 3 along with the second-

☆Grant sponsor: U.S. National Science Foundation; Grant nos. CMMI-0653279, CMMI-1130147.

* Corresponding author.
E-mail addresses: vaibhav-yadav@uiowa.edu (V. Yadav), rahman@engineering.uiowa.edu (S. Rahman).

http://dx.doi.org/10.1016/j.probengmech.2014.08.004
0266-8920/

moment properties of the resultant approximation. Section 4 focuses on the univariate hybrid approximation, resulting in explicit formulae for the hybrid model parameters and second-moment statistics. The mean-squared error analyses pertaining to univariate A-PDD, F-PDD, and hybrid PDD approximations are also discussed. Section 5 explains dimension-reduction integration and the quasi-Monte Carlo method for calculating the PDD expansion coefficients. Section 6 presents two numerical examples for illustrating the accuracy, efficiency, and convergence properties of the hybrid PDD method. In Section 7, a large, complex engineering problem, entailing coupled acoustic-structural analysis of a pickup truck, is solved using the hybrid PDD method. Finally, conclusions are drawn in Section 8.

2. Polynomial dimensional decomposition

Let $\mathbb{N}$, $\mathbb{N}_0$, $\mathbb{R}$, and $\mathbb{R}_0^+$ represent the sets of positive integer (natural), non-negative integer, real, and non-negative real numbers, respectively. For $k \in \mathbb{N}$, denote by $\mathbb{R}^k$ the k-dimensional Euclidean space, by $\mathbb{N}_0^k$ the k-dimensional multi-index space, and by $\mathbb{R}^{k\times k}$ the set of $k\times k$ real-valued matrices. These standard notations will be used throughout the paper.

Let $(\Omega, \mathcal{F}, P)$ be a complete probability space, where Ω is a sample space, $\mathcal{F}$ is a σ-field on Ω, and $P : \mathcal{F} \to [0,1]$ is a probability measure. With $\mathcal{B}^N$ representing the Borel σ-field on $\mathbb{R}^N$, $N \in \mathbb{N}$, consider an $\mathbb{R}^N$-valued random vector $\mathbf{X} := (X_1, \ldots, X_N) : (\Omega, \mathcal{F}) \to (\mathbb{R}^N, \mathcal{B}^N)$, which describes the statistical uncertainties in all system and input parameters of a high-dimensional stochastic problem. The probability law of $\mathbf{X}$ is completely defined by its joint probability density function $f_{\mathbf{X}} : \mathbb{R}^N \to \mathbb{R}_0^+$. Assuming independent coordinates of $\mathbf{X}$, its joint probability density $f_{\mathbf{X}}(\mathbf{x}) = \Pi_{i=1}^{i=N} f_i(x_i)$ is expressed by a product of marginal probability density functions f_i of X_i, $i = 1, \ldots, N$, defined on the probability triple $(\Omega_i, \mathcal{F}_i, P_i)$ with a bounded or an unbounded support on $\mathbb{R}$. For a given $u \subseteq \{1, \ldots, N\}$, $f_{\mathbf{X}_{-u}}(\mathbf{x}_{-u}) := \prod_{i=1, i\notin u}^{N} f_i(x_i)$ defines the marginal density function of $\mathbf{X}_{-u} := \mathbf{X}_{\{1,\ldots,N\}\setminus u}$.

Let $y(\mathbf{X}) := y(X_1, \ldots, X_N)$, a real-valued, measurable transformation on $(\Omega, \mathcal{F})$, define a high-dimensional stochastic response of interest and $\mathcal{L}_2(\Omega, \mathcal{F}, P)$ represent a Hilbert space of square-integrable functions y with respect to the induced generic measure $f_{\mathbf{X}}(\mathbf{x})\, d\mathbf{x}$ supported on $\mathbb{R}^N$. The ANOVA dimensional decomposition (ADD), expressed by the recursive form [8–10]

$$y(\mathbf{X}) = \sum_{u \subseteq \{1,\ldots,N\}} y_u(\mathbf{X}_u), \tag{1}$$

$$y_\varnothing = \int_{\mathbb{R}^N} y(\mathbf{x}) f_{\mathbf{X}}(\mathbf{x})\, d\mathbf{x}, \tag{2}$$

$$y_u(\mathbf{X}_u) = \int_{\mathbb{R}^{N-|u|}} y(\mathbf{X}_u, \mathbf{x}_{-u}) f_{\mathbf{X}_{-u}}(\mathbf{x}_{-u})\, d\mathbf{x}_{-u} - \sum_{v \subset u} y_v(\mathbf{X}_v), \tag{3}$$

is a finite, hierarchical expansion in terms of its input variables with increasing dimensions, where $u \subseteq \{1, \ldots, N\}$ is a subset with the complementary set $-u = \{1, \ldots, N\}\setminus u$ and cardinality $0 \le |u| \le N$, and y_u is a $|u|$-variate component function describing a constant or the interactive effect of $\mathbf{X}_u = (X_{i_1}, \ldots, X_{i_{|u|}})$, $1 \le i_1 < \cdots < i_{|u|} \le N$, a subvector of $\mathbf{X}$, on y when $|u| = 0$ or $|u| > 0$. The summation in Eq. (1) comprises 2^N terms, with each term depending on a group of variables indexed by a particular subset of $\{1, \ldots, N\}$, including the empty set $\varnothing$. In Eq. (3), $(\mathbf{X}_u, \mathbf{x}_{-u})$ denotes an N-dimensional vector whose ith component is X_i if $i \in u$ and x_i if $i \notin u$. When $u = \varnothing$, the sum in Eq. (3) vanishes, resulting in the expression of the constant function $y_\varnothing$ in Eq. (2). When $u = \{1, \ldots, N\}$, the integration in Eq. (3) is on the empty set, reproducing Eq. (1) and hence finding the last function $y_{\{1,\ldots,N\}}$. Indeed, all component functions of y can be obtained by interpreting literally Eq. (3).

The ADD component functions y_u, $u \subseteq \{1, \ldots, N\}$, are uniquely determined from the annihilating conditions [8–10],

$$\int_{\mathbb{R}} y_u(\mathbf{x}_u) f_i(x_i)\, dx_i = 0 \quad \text{for } i \in u, \tag{4}$$

resulting in two remarkable properties: (1) the component functions, y_u, $\varnothing \ne u \subseteq \{1, \ldots, N\}$, have zero means; and (2) two distinct component functions y_u and y_v, where $u \subseteq \{1, \ldots, N\}$, $v \subseteq \{1, \ldots, N\}$, and $u \ne v$, are orthogonal [10]. However, the ADD component functions are difficult to obtain because they require calculation of high-dimensional integrals.

2.1. Additive PDD

Let $\{\psi_{ij}(X_i);\ j = 0, 1, \ldots\}$ be a set of orthonormal polynomial basis functions in the Hilbert space $\mathcal{L}_2(\Omega_i, \mathcal{F}_i, P_i)$ that is consistent with the probability measure P_i of X_i. For a given $\varnothing \ne u = \{i_1, \ldots, i_{|u|}\} \subseteq \{1, \ldots, N\}$, $1 \le |u| \le N$, $1 \le i_1 < \cdots < i_{|u|} \le N$, denote a product probability triple by $(\times_{p=1}^{p=|u|} \Omega_{i_p}, \times_{p=1}^{p=|u|} \mathcal{F}_{i_p}, \times_{p=1}^{p=|u|} P_{i_p})$, and the associated space of square integrable $|u|-$variate component functions of y by $\mathcal{L}_2(\times_{p=1}^{p=|u|} \Omega_{i_p}, \times_{p=1}^{p=|u|} \mathcal{F}_{i_p}, \times_{p=1}^{p=|u|} P_{i_p}) := \{y_u : \int_{\mathbb{R}^{|u|}} y_u^2(\mathbf{x}_u) f_{\mathbf{X}_u}(\mathbf{x}_u)\, d\mathbf{x}_u < \infty\}$, which is a Hilbert space. Since the joint density of $(X_{i_1}, \ldots, X_{i_{|u|}})$ is separable (independence), *i.e.*, $f_{\mathbf{X}_u}(\mathbf{x}_u) = \prod_{p=1}^{|u|} f_{i_p}(x_{i_p})$, the product polynomial $\psi_{u\mathbf{j}_{|u|}}(\mathbf{X}_u) := \prod_{p=1}^{|u|} \psi_{i_p j_p}(X_{i_p})$, where $\mathbf{j}_{|u|} = (j_1, \ldots, j_{|u|}) \in \mathbb{N}_0^{|u|}$, a $|u|-$dimensional multi-index with $\infty-$norm $\|\mathbf{j}_{|u|}\|_\infty := \max(j_1, \ldots, j_{|u|})$, constitutes an orthonormal basis in $\mathcal{L}_2(\times_{p=1}^{p=|u|} \Omega_{i_p}, \times_{p=1}^{p=|u|} \mathcal{F}_{i_p}, \times_{p=1}^{p=|u|} P_{i_p})$. Two important properties of these product polynomials from the tensor product of Hilbert spaces are as follows.

Proposition 1. *The product polynomials $\psi_{u\mathbf{j}_{|u|}}(\mathbf{X}_u)$, $\varnothing \ne u \subseteq \{1, \ldots, N\}$ have zero means, that is,*

$$\mathbb{E}[\psi_{u\mathbf{j}_{|u|}}(\mathbf{X}_u)] = 0. \tag{5}$$

Proposition 2. *Two distinct product polynomials $\psi_{u\mathbf{j}_{|u|}}(\mathbf{X}_u)$ and $\psi_{v\mathbf{k}_{|v|}}(\mathbf{X}_v)$, where $\varnothing \ne u \subseteq \{1, \ldots, N\}$, $\varnothing \ne v \subseteq \{1, \ldots, N\}$, $j_1, \ldots, j_{|u|} \ne 0$, $k_1, \ldots, k_{|v|} \ne 0$, are uncorrelated and each has unit variance, that is,*

$$\mathbb{E}[\psi_{u\mathbf{j}_{|u|}}(\mathbf{X}_u)\psi_{v\mathbf{k}_{|v|}}(\mathbf{X}_v)] = \begin{cases} 1 & \text{if } u = v;\ \mathbf{j}_{|u|} = \mathbf{k}_{|v|}, \\ 0 & \text{otherwise.} \end{cases} \tag{6}$$

From the standard Hilbert space theory, every non-constant component function $y_u \in \mathcal{L}_2(\times_{p=1}^{p=|u|} \Omega_{i_p}, \times_{p=1}^{p=|u|} \mathcal{F}_{i_p}, \times_{p=1}^{p=|u|} P_{i_p})$ of y can be expanded as [1,2]

$$y_u(\mathbf{X}_u) = \sum_{\substack{\mathbf{j}_{|u|} \in \mathbb{N}_0^{|u|} \\ j_1 \cdots j_{|u|} \ne 0}} C_{u\mathbf{j}_{|u|}} \psi_{u\mathbf{j}_{|u|}}(\mathbf{X}_u), \quad \varnothing \ne u \subseteq \{1, \ldots, N\}, \tag{7}$$

with

$$C_{u\mathbf{j}_{|u|}} := \int_{\mathbb{R}^N} y(\mathbf{x}) \psi_{u\mathbf{j}_{|u|}}(\mathbf{x}_u) f_{\mathbf{X}}(\mathbf{x})\, d\mathbf{x}, \quad \varnothing \ne u \subseteq \{1, \ldots, N\},\ \mathbf{j}_{|u|} \in \mathbb{N}_0^{|u|}, \tag{8}$$

representing the corresponding expansion coefficient. Note that the summation in Eq. (7) precludes $j_1, \ldots, j_{|u|} = 0$, that is, the individual degree of each variable X_i in $\psi_{u\mathbf{j}_{|u|}}$, $i \in u$, cannot be *zero* since y_u is a strictly $|u|$-variate function and has a *zero* mean. The end result of combining Eqs. (1) and (7) is the A-PDD [1,2]

$$y(\mathbf{X}) = y_\varnothing + \sum_{\varnothing \ne u \subseteq \{1,\ldots,N\}} \sum_{\substack{\mathbf{j}_{|u|} \in \mathbb{N}_0^{|u|} \\ j_1 \cdots j_{|u|} \ne 0}} C_{u\mathbf{j}_{|u|}} \psi_{u\mathbf{j}_{|u|}}(\mathbf{X}_u), \tag{9}$$

providing an exact, hierarchical expansion of y in terms of an infinite number of coefficients or orthonormal polynomials. Using Propositions 1 and 2, all component functions y_u, $\varnothing \neq u \subseteq \{1,\ldots,N\}$, in Eq. (7) are found to satisfy the annihilating conditions of the ADD. Therefore, A-PDD can be viewed as the polynomial version of ADD and is, therefore, endowed with all desirable properties of ADD.

In many physical and engineering applications, the function y can be approximated by a sum of at most S-variate component functions, where $1 \le S \le N$, resulting in the S-variate, mth-order A-PDD approximation

$$\tilde{y}_{S,m}(\mathbf{X}) = y_{\varnothing} + \sum_{\substack{\varnothing \neq u \subseteq \{1,\ldots,N\} \\ 1 \le |u| \le S}} \sum_{\substack{\mathbf{j}_{|u|} \in \mathbb{N}_0^{|u|}, \|\mathbf{j}_{|u|}\|_\infty \le m \\ j_1 \cdots j_{|u|} \neq 0}} C_{u\mathbf{j}_{|u|}} \psi_{u\mathbf{j}_{|u|}}(\mathbf{X}_u), \tag{10}$$

containing $\sum_{k=0}^{S} \binom{N}{S-k} m^{S-k}$ number of A-PDD coefficients and corresponding orthonormal polynomials. Due to its additive structure, the approximation in Eq. (10) includes degrees of interaction among at most S input variables $X_{i_1},\ldots,X_{i_S}$, $1 \le i_1 \le \cdots \le i_S \le N$. For instance, by selecting $S=1$ and 2, the functions $\tilde{y}_{1,m}$ and $\tilde{y}_{2,m}$, respectively, provide univariate and bivariate mth-order approximations, contain contributions from all input variables, and should not be viewed as first- and second-order approximations, nor do they limit the nonlinearity of y. Depending on how the component functions are constructed, arbitrarily high-order univariate and bivariate terms of y could be lurking inside $\tilde{y}_{1,m}$ and $\tilde{y}_{2,m}$. When $S \to N$ and $m \to \infty$, $\tilde{y}_{S,m}$ converges to y in the mean-square sense, permitting Eq. (10) to generate a hierarchical and convergent sequence of approximations of y.

Applying the expectation operator on $\tilde{y}_{S,m}(\mathbf{X})$ and $(\tilde{y}_{S,m}(\mathbf{X}) - y_{\varnothing})^2$ and noting Propositions 1 and 2, the mean [11]

$$\mathbb{E}[\tilde{y}_{S,m}(\mathbf{X})] = y_{\varnothing} \tag{11}$$

of the S-variate, mth-order A-PDD approximation matches the exact mean $\mathbb{E}[y(\mathbf{X})]$, regardless of S or m, and the approximate variance [11]

$$\begin{aligned} \tilde{\sigma}^2_{S,m} &:= \mathbb{E}[(\tilde{y}_{S,m}(\mathbf{X}) - \mathbb{E}[\tilde{y}_{S,m}(\mathbf{X})])^2] \\ &= \sum_{\substack{\varnothing \neq u \subseteq \{1,\ldots,N\} \\ 1 \le |u| \le S}} \sum_{\substack{\mathbf{j}_{|u|} \in \mathbb{N}_0^{|u|}, \|\mathbf{j}_{|u|}\|_\infty \le m \\ j_1 \cdots j_{|u|} \neq 0}} C^2_{u\mathbf{j}_{|u|}} \end{aligned} \tag{12}$$

is calculated as the sum of squares of the expansion coefficients from the S-variate, mth-order A-PDD approximation of $y(\mathbf{X})$. It is elementary to show that the approximate variance in Eq. (12) approaches the exact variance of y when $S \to N$ and $m \to \infty$ [11]. The mean-square convergence of $\tilde{y}_{S,m}$ is guaranteed as y, and its component functions are all members of the associated Hilbert spaces.

For the special case of $S=1$, the univariate A-PDD approximation

$$\tilde{y}_{1,m}(\mathbf{X}) = y_{\varnothing} + \sum_{i=1}^{N} \sum_{j=1}^{m} C_{ij} \psi_{ij}(X_i) \tag{13}$$

of $y(\mathbf{X})$ yields the exact mean

$$\mathbb{E}\left[\tilde{y}_{1,m}(\mathbf{X})\right] = y_{\varnothing}, \tag{14}$$

and an approximate variance

$$\tilde{\sigma}^2_{1,m} := \mathbb{E}[(\tilde{y}_{1,m}(\mathbf{X}) - \mathbb{E}[\tilde{y}_{1,m}(\mathbf{X})])^2] = \sum_{i=1}^{N} \sum_{j=1}^{m} C^2_{ij} \tag{15}$$

that depends on $m < \infty$.

2.2. Factorized PDD

The factorized dimensional decomposition of the multivariate function

$$y(\mathbf{X}) = \prod_{u \subseteq \{1,\ldots,N\}} [1 + z_u(\mathbf{X}_u)], \tag{16}$$

where z_u, $u \subseteq \{1,\ldots,N\}$, are various component functions of input variables with increasing dimensions. Like the sum in Eq. (1), the product in Eq. (16) comprises 2^N terms, with each term depending on a group of variables indexed by a particular subset of $\{1,\ldots,N\}$, including the empty set $\varnothing$. This multiplicative decomposition exists and is unique for any square-integrable function $y \in \mathcal{L}_2(\Omega, \mathcal{F}, P)$ with a non-zero mean. Tunga and Demiralp [12] originally proposed this decomposition, calling it factorized high-dimensional model representation. Subsequently, Yadav and Rahman [7], and Rahman [13] derived a recursive relationship between the component functions of ANOVA and factorized dimensional decompositions, as described by Theorem 1, leading to F-PDD.

Theorem 1. *The recursive relationships between component functions of the ANOVA and factorized dimensional decompositions of a non-zero mean, square-integrable function $y : \mathbb{R}^N \to \mathbb{R}$, represented by Eqs. (1) and (16), respectively, are*

$$1 + z_u(\mathbf{X}_u) = \frac{\sum_{v \subseteq u} y_v(\mathbf{X}_v)}{\prod_{v \subset u} [1 + z_v(\mathbf{X}_v)]}, \quad u \subseteq \{1,\ldots,N\}. \tag{17}$$

Proof. See Theorem 8 of Yadav and Rahman [7] or Theorem 3.4 of Rahman [13]. □

Applying Eq. (7) into Eq. (17) and then combining with Eq. (16) form the F-PDD of

$$y(\mathbf{X}) = y_{\varnothing} \prod_{\varnothing \neq u \subseteq \{1,\ldots,N\}} \left[\frac{y_{\varnothing} + \sum_{\varnothing \neq v \subseteq u} \sum_{\substack{\mathbf{j}_{|v|} \in \mathbb{N}_0^{|v|} \\ j_1 \cdots j_{|v|} \neq 0}} C_{v\mathbf{j}_{|v|}} \psi_{v\mathbf{j}_{|v|}}(\mathbf{X}_v)}{\prod_{v \subset u} [1 + z_v(\mathbf{X}_v)]} \right], \tag{18}$$

as an exact representation of $y(\mathbf{X})$, where infinite orthonormal polynomials of increasing dimensions are structured with a multiplicative hierarchy, as opposed to the additive hierarchy in Eq. (9). Consequently, an S-variate, mth-order F-PDD approximation, retaining at most S-variate component functions and mth-order orthogonal polynomials, becomes

$$\hat{y}_{S,m}(\mathbf{X}) = y_{\varnothing} \prod_{\substack{\varnothing \neq u \subseteq \{1,\ldots,N\} \\ 1 \le |u| \le S}} \left[\frac{y_{\varnothing} + \sum_{\varnothing \neq v \subseteq u} \sum_{\substack{\mathbf{j}_{|v|} \in \mathbb{N}_0^{|v|}, \|\mathbf{j}_{|u|}\|_\infty \le m \\ j_1 \cdots j_{|v|} \neq 0}} C_{v\mathbf{j}_{|v|}} \psi_{v\mathbf{j}_{|v|}}(\mathbf{X}_v)}{\prod_{v \subset u} [1 + z_v(\mathbf{X}_v)]} \right]. \tag{19}$$

It is elementary to show that the S-variate, mth-order F-PDD approximation converges to $y(\mathbf{X})$ in the mean-square sense when $S \to N$ and $m \to \infty$.

Unlike Eqs. (11) and (12), the mean and variance of $\hat{y}_{S,m}(\mathbf{X})$, respectively defined as

$$\mathbb{E}[\hat{y}_{S,m}(\mathbf{X})] := \int_{\mathbb{R}^N} \hat{y}_{S,m}(\mathbf{x}) f_{\mathbf{X}}(\mathbf{x})\, d\mathbf{x} \tag{20}$$

and

$$\begin{aligned} \hat{\sigma}^2_{S,m} &:= \mathbb{E}[(\hat{y}_{S,m}(\mathbf{X}) - \mathbb{E}[\hat{y}_{S,m}(\mathbf{X})])^2] \\ &:= \int_{\mathbb{R}^N} (\hat{y}_{S,m}(\mathbf{x}) - \mathbb{E}[\hat{y}_{S,m}(\mathbf{X})])^2 f_{\mathbf{X}}(\mathbf{x})\, d\mathbf{x}, \end{aligned} \tag{21}$$

do not produce closed-form or analytic expressions in terms of $y_{\varnothing}$

and $C_{u\mathbf{j}_{|u|}}$ if S is selected arbitrarily. This is a drawback of F-PDD when compared with A-PDD. Having said so, they are easily estimated by sampling methods, such as quasi- and crude Monte Carlo simulations (MCSs), or even numerical integration if N is not overly large.

When $S=1$, the univariate F-PDD approximation

$$\hat{y}_{1,m}(\mathbf{X}) = y_{\varnothing}\left[\prod_{i=1}^{N}\left\{1+\frac{1}{y_{\varnothing}}\sum_{j=1}^{m}C_{ij}\psi_{ij}(X_i)\right\}\right], \tag{22}$$

forms a product of univariate polynomials. Eq. (22) results in the exact mean

$$\mathbb{E}[\hat{y}_{1,m}(\mathbf{X})] = y_{\varnothing}, \tag{23}$$

and an approximate variance

$$\begin{aligned}\hat{\sigma}^2_{1,m} &:= \mathbb{E}[(\hat{y}_{1,m}(\mathbf{X}) - \mathbb{E}[\hat{y}_{1,m}(\mathbf{X})])^2] \\ &= y_{\varnothing}^2\left[\prod_{i=1}^{N}\left(1+\frac{1}{y_{\varnothing}^2}\sum_{j=1}^{m}C_{ij}^2\right)-1\right]\end{aligned} \tag{24}$$

that are valid for an arbitrary $m<\infty$.

3. Hybrid PDD

When a desired stochastic response exhibits neither a dominantly additive nor a dominantly multiplicative nature, then a mixed approach that optimally combines A-PDD and F-PDD approximations is needed. Two linear hybrid approximations are proposed.

3.1. Hybrid approximations

Given S-variate, mth-order additive PDD and factorized PDD approximations $\tilde{y}_{S,m}(\mathbf{X})$ and $\hat{y}_{S,m}(\mathbf{X})$, let

$$\begin{aligned}&\overline{y}_{S,m}(\mathbf{X};\alpha_{S,m},\beta_{S,m},\ldots) \\ &:= \begin{cases} y_{\varnothing} & \text{if } S=0, \\ h(\tilde{y}_{S,m}(\mathbf{X}),\hat{y}_{S,m}(\mathbf{X});\alpha_{S,m},\beta_{S,m},\ldots) & \text{if } 1\le S<N, \\ y(\mathbf{X}) & \text{if } S=N,\ m\to\infty, \end{cases}\end{aligned} \tag{25}$$

define a general, S-variate, mth-order hybrid PDD approximation of $y(\boldsymbol{X})$, where h is a chosen model function such that $\mathbb{E}[\overline{y}_{S,m}(\mathbf{X};\alpha_{S,m},\beta_{S,m},\ldots)] = y_{\varnothing}$ and $\alpha_{S,m}$, $\beta_{S,m},\ldots$ are the associated model parameters. Define the *zero*-mean functions

$$w(\mathbf{X}) := y(\mathbf{X}) - y_{\varnothing}, \tag{26}$$

$$\tilde{w}_{S,m}(\mathbf{X}) := \tilde{y}_{S,m}(\mathbf{X}) - y_{\varnothing}, \tag{27}$$

$$\hat{w}_{S,m}(\mathbf{X}) := \hat{y}_{S,m}(\mathbf{X}) - \mathbb{E}[\hat{y}_{S,m}(\mathbf{X})], \tag{28}$$

and

$$\overline{w}_{S,m}(\mathbf{X};\alpha_{S,m},\beta_{S,m},\ldots) := \overline{y}_{S,m}(\mathbf{X};\alpha_{S,m},\beta_{S,m},\ldots) - y_{\varnothing}, \tag{29}$$

that will be used throughout this section. Theorem 2 and Corollary 1 describe two optimal linear hybrid approximations $\overline{y}_{S,m}(\mathbf{X};\alpha_{S,m},\beta_{S,m})$ and $\overline{y}'_{S,m}(\mathbf{X};\alpha'_{S,m},\beta'_{S,m})$ for $1\le S<N$, $m<\infty$, both producing the exact mean $y_{\varnothing}$. The two hybrid approximations have their *zero*-mean counterparts defined as

$$\overline{w}_{S,m}(\mathbf{X};\alpha_{S,m},\beta_{S,m}) := \overline{y}_{S,m}(\mathbf{X};\alpha_{S,m},\beta_{S,m}) - y_{\varnothing} \tag{30}$$

and

$$\overline{w}'_{S,m}(\mathbf{X};\alpha'_{S,m}) := \overline{y}'_{S,m}(\mathbf{X};\alpha'_{S,m}) - y_{\varnothing}. \tag{31}$$

Theorem 2. *Given integers* $1\le S<N<\infty$ *and* $1\le m<\infty$, *let* $\tilde{w}_{S,m}(\mathbf{X})$ *and* $\hat{w}_{S,m}(\mathbf{X})$ *represent zero-mean, S-variate, mth-order additive PDD and factorized PDD approximations with variances* $\tilde{\sigma}^2_{S,m} := \mathbb{E}[\tilde{y}_{S,m}(\mathbf{X}) - y_{\varnothing}]^2 = \mathbb{E}[\tilde{w}^2_{S,m}(\mathbf{X})]$ *and* $\hat{\sigma}^2_{S,m} := \mathbb{E}[\hat{y}_{S,m}(\mathbf{X}) - y_{\varnothing}]^2 = \mathbb{E}[\hat{w}^2_{S,m}(\mathbf{X})]$, *respectively, of a real-valued, zero-mean, square-integrable function* $w(\mathbf{X})$. *Then there exists an optimal, linear, S-variate, mth-order hybrid PDD approximation*

$$\overline{w}_{S,m}(\mathbf{X};\alpha_{S,m},\beta_{S,m}) = \alpha_{S,m}\tilde{w}_{S,m}(\mathbf{X}) + \beta_{S,m}\hat{w}_{S,m}(\mathbf{X}) \tag{32}$$

of $w(\mathbf{X})$, *where*

$$\alpha_{S,m} = \frac{\hat{\sigma}^2_{S,m}\mathbb{E}[w(\mathbf{X})\tilde{w}_{S,m}(\mathbf{X})] - \mathbb{E}[\tilde{w}_{S,m}(\mathbf{X})\hat{w}_{S,m}(\mathbf{X})]\mathbb{E}[w(\mathbf{X})\hat{w}_{S,m}(\mathbf{X})]}{\tilde{\sigma}^2_{S,m}\hat{\sigma}^2_{S,m} - (\mathbb{E}[\tilde{w}_{S,m}(\mathbf{X})\hat{w}_{S,m}(\mathbf{X})])^2}, \tag{33}$$

$$\beta_{S,m} = \frac{\tilde{\sigma}^2_{S,m}\mathbb{E}[w(\mathbf{X})\hat{w}_{S,m}(\mathbf{X})] - \mathbb{E}[\tilde{w}_{S,m}(\mathbf{X})\hat{w}_{S,m}(\mathbf{X})]\mathbb{E}[w(\mathbf{X})\tilde{w}_{S,m}(\mathbf{X})]}{\tilde{\sigma}^2_{S,m}\hat{\sigma}^2_{S,m} - (\mathbb{E}[\tilde{w}_{S,m}(\mathbf{X})\hat{w}_{S,m}(\mathbf{X})])^2}. \tag{34}$$

Proof. For a square-integrable function $w(\mathbf{X})$, define a second-moment error

$$\overline{e}_{S,m} := \mathbb{E}[w(\mathbf{X}) - \overline{w}_{S,m}(\mathbf{X};\alpha_{S,m},\beta_{S,m})]^2 \tag{35}$$

committed by its S-variate, mth-order hybrid PDD approximation $\overline{w}_{S,m}(\mathbf{X};\alpha_{S,m},\beta_{S,m})$. For $\overline{e}_{S,m}$ to be minimum, set

$$\begin{aligned}\frac{\partial\overline{e}_{S,m}}{\partial\alpha_{S,m}} &= 0, \\ \frac{\partial\overline{e}_{S,m}}{\partial\beta_{S,m}} &= 0.\end{aligned} \tag{36}$$

Exchanging the orders of differential and expectation operators and substituting the expression of $\overline{w}_{S,m}(\mathbf{X};\alpha_{S,m},\beta_{S,m})$ from Eq. (32) yield

$$\begin{aligned}\alpha_{S,m}\mathbb{E}[\tilde{w}^2_{S,m}(\mathbf{X})] + \beta_{S,m}\mathbb{E}[\tilde{w}_{S,m}(\mathbf{X})\hat{w}_{S,m}(\mathbf{X})] &= \mathbb{E}[w(\mathbf{X})\tilde{w}_{S,m}(\mathbf{X})], \\ \alpha_{S,m}\mathbb{E}[\tilde{w}_{S,m}(\mathbf{X})\hat{w}_{S,m}(\mathbf{X})] + \beta_{S,m}\mathbb{E}[\hat{w}^2_{S,m}(\mathbf{X})] &= \mathbb{E}[w(\mathbf{X})\hat{w}_{S,m}(\mathbf{X})].\end{aligned} \tag{37}$$

Noting $\tilde{\sigma}^2_{S,m} = \mathbb{E}[\tilde{w}^2_{S,m}(\mathbf{X})]$ and $\hat{\sigma}^2_{S,m} = \mathbb{E}[\hat{w}^2_{S,m}(\mathbf{X})]$, the solution of equations (37) produces the expressions of $\alpha_{S,m}$ and $\beta_{S,m}$ as in Eqs. (33) and (34), thus proving the theorem. □

Corollary 1. *Constraining the sum of two model parameters to be unity in Eqs.* (32) *through* (37) *creates another optimal, linear, S-variate hybrid approximation*

$$\overline{w}'_{S,m}(\mathbf{X};\alpha'_{S,m}) = \alpha'_{S,m}\tilde{w}_{S,m}(\mathbf{X}) + (1-\alpha'_{S,m})\hat{w}_{S,m}(\mathbf{X}) \tag{38}$$

of $w(\mathbf{X})$, $1\le S<N<\infty$, $m<\infty$, *where the optimal model parameter*

$$\alpha'_{S,m} = \frac{\mathbb{E}[\{w(\mathbf{X})-\hat{w}_{S,m}(\mathbf{X})\}\{\tilde{w}_{S,m}(\mathbf{X})-\hat{w}_{S,m}(\mathbf{X})\}]}{\mathbb{E}[\tilde{w}_{S,m}(\mathbf{X})-\hat{w}_{S,m}(\mathbf{X})]^2}. \tag{39}$$

Proof. For a square-integrable function $w(\mathbf{X})$, define another second-moment error

$$\overline{e}'_{S,m} := \mathbb{E}[w(\mathbf{X}) - \overline{w}'_{S,m}(\mathbf{X};\alpha'_{S,m})]^2 \tag{40}$$

owing to its S-variate, mth-order hybrid PDD approximation $\overline{w}'_{S,m}(\mathbf{X};\alpha'_{S,m})$. For $\overline{e}'_{S,m}$ to be minimum, set

$$\frac{\partial\overline{e}'_{S,m}}{\partial\alpha'_{S,m}} = 0. \tag{41}$$

Again, swapping the orders of differential and expectation operators, and substituting the expression of $\overline{w}'_{S,m}(\mathbf{X};\alpha'_{S,m})$ from Eq. (38) result in the expression of $\alpha'_{S,m}$ as in Eq. (39), thus proving the corollary. □

Remark 1. The second hybrid approximation $\overline{w}'_{S,m}$ for $S=1$ or 2 presented in Corollary 1 coincides with that proposed by Tunga and Demiralp [12]. However, the first hybrid approximation $\overline{w}_{S,m}$ – that is, Theorem 2 – is new. Furthermore, the two approximations, $\overline{w}_{S,m}$ and $\overline{w}'_{S,m}$, are not the same for a general truncation $2\le S<N$. See a recent work of Rahman [13] for distinction between these

two linear models, including a nonlinear variant, not discussed in this paper for brevity.

Remark 2. The hybrid PDD approximations exist for any function y or w with a finite variance. The approximations, $\overline{w}_{S,m}(\mathbf{X};\alpha_{S,m},\beta_{S,m})$ and $\overline{w}'_{S,m}(\mathbf{X};\alpha'_{S,m})$, for a given $1\le S<N<\infty$, and $1\le m<\infty$, can exactly reproduce the original *zero*-mean function $w(\mathbf{X})$ under the following two conditions: (1) if the original function is endowed with a purely additive structure, i.e., $w(\mathbf{X})=\tilde{w}_{S,m}(\mathbf{X})$, then Eqs. (33), (34), and (39) yield $\alpha_{S,m}=\alpha'_{S,m}=1$, and $\beta_{S,m}=0$, which in turn results in $\overline{w}_{S,m}(\mathbf{X})=\overline{w}'_{S,m}(\mathbf{X})=\tilde{w}_{S,m}(\mathbf{X})=w(\mathbf{X})$; (2) if the original function possesses a purely multiplicative structure, i.e., $w(\mathbf{X})=\hat{w}_{S,m}(\mathbf{X})$, then Eqs. (33), (34), and (39) produce $\alpha_{S,m}=\alpha'_{S,m}=0$ and $\beta_{S,m}=1$, and therefore $\overline{w}_{S,m}(\mathbf{X})=\overline{w}'_{S,m}(\mathbf{X})=\hat{w}_{S,m}(\mathbf{X})=w(\mathbf{X})$.

3.2. Second-moment properties

Applying the expectation operator on Eqs. (32) and (38) yields the exact mean

$$\mathbb{E}[\overline{y}_{S,m}(\mathbf{X};\alpha_{S,m},\beta_{S,m})]=\mathbb{E}[\overline{y}'_{S,m}(\mathbf{X};\alpha'_{S,m})]=y_{\varnothing}, \tag{42}$$

by both the hybrid approximations. However, their respective variances, obtained by applying the expectation operator on $\overline{w}_{S,m}(\mathbf{X};\alpha_{S,m},\beta_{S,m})^2$ and $\overline{w}'_{S,m}(\mathbf{X};\alpha'_{S,m},\beta'_{S,m})^2$, respectively, vary according to

$$\begin{aligned}\overline{\sigma}^2_{S,m}&:=\mathbb{E}[\overline{w}^2_{S,m}(\mathbf{X};\alpha_{S,m},\beta_{S,m})]\\&=\alpha^2_{S,m}\tilde{\sigma}^2_{S,m}+\beta^2_{S,m}\hat{\sigma}^2_{S,m}+2\alpha_{S,m}\beta_{S,m}\mathbb{E}[\tilde{w}_{S,m}(\mathbf{X})\hat{w}_{S,m}(\mathbf{X})]\end{aligned} \tag{43}$$

and

$$\begin{aligned}\overline{\sigma}'^2_{S,m}&:=\mathbb{E}[\overline{w}'^2_{S,m}(\mathbf{X};\alpha'_{S,m})]\\&=\alpha'^2_{S,m}\tilde{\sigma}^2_{S,m}+(1-\alpha'_{S,m})^2\hat{\sigma}^2_{S,m}+2\alpha'_{S,m}(1-\alpha'_{S,m})\mathbb{E}[\tilde{w}_{S,m}(\mathbf{X})\hat{w}_{S,m}(\mathbf{X})].\end{aligned} \tag{44}$$

Compared with the additive and factorized PDD approximations, the hybrid PDD approximations proposed require expectation of product of $\tilde{w}_{S,m}(\mathbf{X})$ and $\hat{w}_{S,m}(\mathbf{X})$ to calculate the variance.

4. Univariate hybrid PDD approximation

At the root of developing the PDD methods lies the principal motive of achieving high accuracy in calculating the probabilistic characteristics of high-dimensional random responses while keeping the computational efforts to a minimum. This objective was attained through foresaking the inefficient higher-variate expansions and applying only univariate hybrid PDD approximations in solving high-dimensional stochastic problems. Considering the key advantage of high efficiency of a univariate additive [1] and factorized PDD [7] approximations, only the univariate hybrid PDD method was implemented in this work. Proposition 3 formally describes the univariate hybrid PDD approximation.

Proposition 3. *A linear, univariate, mth-order hybrid PDD approximation of $w(\mathbf{X})$, obtained by setting $S=1$ in Eqs. (32)–(34), is*

$$\overline{w}_{1,m}(\mathbf{X};\alpha_{1,m},\beta_{1,m})=\alpha_{1,m}\tilde{w}_{1,m}(\mathbf{X})+\beta_{1,m}\hat{w}_{1,m}(\mathbf{X}) \tag{45}$$

where the model parameters

$$\alpha_{1,m}=\frac{\hat{\sigma}^2_{1,m}-\mathbb{E}[w(\mathbf{X})\hat{w}_{1,m}(\mathbf{X})]}{\hat{\sigma}^2_{1,m}-\tilde{\sigma}^2_{1,m}} \tag{46}$$

and

$$\beta_{1,m}=\frac{\mathbb{E}[w(\mathbf{X})\hat{w}_{1,m}(\mathbf{X})]-\tilde{\sigma}^2_{1,m}}{\hat{\sigma}^2_{1,m}-\tilde{\sigma}^2_{1,m}}. \tag{47}$$

Proof. Consider the univariate, mth-order additive and factorized PDD approximations

$$\tilde{w}_{1,m}(\mathbf{X})=\sum_{i=1}^{N}\sum_{j=1}^{m}C_{ij}\psi_{ij}(X_i), \tag{48}$$

$$\hat{w}_{1,m}(\mathbf{X})=y_{\varnothing}\left[\prod_{i=1}^{N}\left\{1+\frac{1}{y_{\varnothing}}\sum_{j=1}^{m}C_{ij}\psi_{ij}(X_i)\right\}\right]-y_{\varnothing}, \tag{49}$$

of

$$w(\mathbf{X})=\sum_{\varnothing\neq u\subseteq\{1,\ldots,N\}}\sum_{\substack{\mathbf{j}_{|u|}\in\mathbb{N}_0^{|u|}\\ j_1,\ldots,j_{|u|}\neq 0}}C_{u\mathbf{j}_{|u|}}\psi_{u\mathbf{j}_{|u|}}(\mathbf{X}_u). \tag{50}$$

From Propositions 1 and 2,

$$\begin{aligned}\mathbb{E}[w(\mathbf{X})\tilde{w}_{1,m}(\mathbf{X})]&=\mathbb{E}[\tilde{w}_{1,m}(\mathbf{X})\hat{w}_{1,m}(\mathbf{X})]\\&=\sum_{i=1}^{N}\sum_{j=1}^{m}C^2_{ij}=\tilde{\sigma}^2_{1,m}.\end{aligned} \tag{51}$$

Applying Eq. (51) to Eqs. (33) and (34), the model parameters for $S=1$ and $m<\infty$ are obtained as in Eqs. (46) and (47). □

Remark 3. The two parameters $\alpha_{1,m}$ and $\beta_{1,m}$ of the hybrid model described by Eq. (45) add up to one. This is due to special properties of $\tilde{w}_{1,m}(\mathbf{X})$ and $\hat{w}_{1,m}(\mathbf{X})$ expressed in Eqs. (48) and (49). Therefore, the hybrid model described by Eq. (38) at univariate truncation ($S=1$) is redundant, as it leads to the same solution of the first model described by Eq. (45).

Since $\beta_{1,m}=1-\alpha_{1,m}$, let

$$\begin{aligned}\overline{w}_{1,m}(\mathbf{X};\alpha_{1,m})&:=\overline{y}_{1,m}(\mathbf{X};\alpha_{1,m})-y_{\varnothing}\\&=\alpha_{1,m}\tilde{w}_{1,m}(\mathbf{X})+(1-\alpha_{1,m})\hat{w}_{1,m}(\mathbf{X})\end{aligned} \tag{52}$$

denote the univariate hybrid PDD approximation of $w(\mathbf{X})$. The mean of $\overline{w}_{1,m}(\mathbf{X};\alpha_{1,m})$ is *zero* and, therefore, $\mathbb{E}[\overline{y}_{1,m}(\mathbf{X};\alpha_{1,m})]=y_{\varnothing}$, matching the exact mean of $y(\mathbf{X})$. The variance of $\overline{w}_{1,m}(\mathbf{X};\alpha_{1,m})$ or $\overline{y}_{1,m}(\mathbf{X};\alpha_{1,m})$ is

$$\begin{aligned}\overline{\sigma}^2_{1,m}&:=\mathbb{E}[\overline{w}^2_{1,m}(\mathbf{X};\alpha_{1,m})]\\&=(2\alpha_{1,m}-\alpha^2_{1,m})\tilde{\sigma}^2_{1,m}+(1-\alpha_{1,m})^2\hat{\sigma}^2_{1,m},\end{aligned} \tag{53}$$

which is a linear combination of the variances from univariate additive PDD and univariate factorized PDD approximations. The variances $\tilde{\sigma}^2_{1,m}$ and $\hat{\sigma}^2_{1,m}$, expressed by Eqs. (15) and (24), are obtained from the univariate PDD expansion coefficients. However, determining the model parameter $\alpha_{1,m}$ involves evaluation of an N-dimensional integral that will incur additional computational expense in excess of the computations performed for estimating the PDD expansion coefficients. A quasi-MCS was employed for estimating the model parameters, described as follows.

4.1. Calculation of the hybrid model parameter

The basic idea of a quasi-MCS is to replace the random or pseudo-random samples in crude MCS by well-chosen deterministic samples that are highly equidistributed [14]. The quasi-MCS samples are often selected from a low-discrepancy sequence [14–17] or by lattice rules [18] to minimize the integration errors. The estimation of the expectation of the multi-variate function $w(\mathbf{X})\hat{w}_{1,m}(\mathbf{X})$, which is a high-dimensional integral, comprises three simple steps: (1) generate a low-discrepancy point set $\mathcal{P}_L:=\{\mathbf{u}^{(k)}\in[0,1]^N,\ k=1,\ldots,L\}$ of size $L\in\mathbb{N}$; (2) map each sample from $\mathcal{P}_L$ to the sample $\mathbf{x}^{(k)}\in\mathbb{R}^N$ following the probability measure of the random input $\mathbf{X}$; and (3) approximate the expectation as $\mathbb{E}[w(\mathbf{X})\hat{w}_{1,m}(\mathbf{X})]\cong(1/L)\sum_{k=1}^{L}[w(\mathbf{x}^{(k)})\hat{w}_{1,m}(\mathbf{x}^{(k)})]$. Thus, using quasi-MCS, the model

parameter is given by

$$\alpha_{1,m} \cong \frac{\hat{\sigma}^2_{1,m} - \frac{1}{L}\sum_{k=1}^{L}[w(\mathbf{x}^{(k)})\hat{w}_{1,m}(\mathbf{x}^{(k)})]}{\hat{\sigma}^2_{1,m} - \tilde{\sigma}^2_{1,m}}, \tag{54}$$

where $\hat{\sigma}^2_{1,m}$ and $\tilde{\sigma}^2_{1,m}$ are obtained from Eqs. (15) and (24). However, when $\hat{\sigma}^2_{1,m} = \mathbb{E}[\hat{w}^2_{1,m}(\mathbf{X})]$ and $\tilde{\sigma}^2_{1,m} = \mathbb{E}[\tilde{w}^2_{1,m}(\mathbf{X})]$ are also estimated from a quasi-MCS method, then the model parameter can also be obtained from

$$\alpha_{1,m} \cong \frac{\frac{1}{L}\sum_{k=1}^{L}[\hat{w}^2_{1,m}(\mathbf{x}^{(k)})] - \frac{1}{L}\sum_{k=1}^{L}[w(\mathbf{x}^{(k)})\hat{w}_{1,m}(\mathbf{x}^{(k)})]}{\frac{1}{L}\sum_{k=1}^{L}[\hat{w}^2_{1,m}(\mathbf{x}^{(k)})] - \frac{1}{L}\sum_{k=1}^{L}[\tilde{w}^2_{1,m}(\mathbf{x}^{(k)})]}. \tag{55}$$

The well-known Koksma–Hlawka inequality reveals that the error committed by a quasi-MCS is bounded by the variation of the integrand in the sense of Hardy and Krause and the star-discrepancy, a measure of uniformity, of the point set $\mathcal{P}_L$ [14]. Therefore, constructing a point set with star-discrepancy as small as possible and seeking variance reduction of the integrand are vital for the success of the quasi-MCS. It should be mentioned here that many authors, including Halton [15], Faure [16], Niederreiter [14], Sobol [17], and Wang [19], have extensively studied how to generate the best low-discrepancy point sets and sequences and to engender variance reduction. For a bounded variation of the integrand, the quasi-MCS has a theoretical error bound $O(L^{-1}(\log L)^N$ compared with the probabilistic error bound $O(N^{-1/2})$ of crude MCS, indicating significantly faster convergence of the quasi-MCS than crude MCS.

Both Eqs. (54) and (55) were employed for estimating $\alpha_{1,m}$ in this work. Further details, clarifying which equation is used, are given in the Numerical Examples section.

4.2. Error analysis

Given the univariate truncation ($S = 1$), which approximation stemming from additive PDD, factorized PDD, and hybrid PDD is more accurate? Lemma 1 and Theorem 3 address this question.

Lemma 1. *Given an integer $1 \le m < \infty$, the variance of the univariate factorized PDD approximation $\hat{y}_{1,m}(\mathbf{X})$ is greater than or equal to the variance of the univariate additive PDD approximation $\tilde{y}_{1,m}(\mathbf{X})$, that is,*

$$\hat{\sigma}^2_{1,m} \ge \tilde{\sigma}^2_{1,m}.$$

Proof. From Eq. (24),

$$\begin{aligned}\hat{\sigma}^2_{1,m} &= y^2_{\varnothing}\left[\prod_{i=1}^{N}\left(1+\frac{1}{y^2_{\varnothing}}\sum_{j=1}^{m} C^2_{ij}\right)-1\right] \\ &= \sum_{i=1}^{N}\sum_{j=1}^{m} C^2_{ij} + y^2_{\varnothing}\sum_{s=2}^{N}\sum_{\varnothing \ne u \subseteq \{1,\ldots,N\} \atop |u|=s}\prod_{i\in u}\frac{1}{y^2_{\varnothing}}\sum_{j=1}^{m} C^2_{ij} \\ &\ge \tilde{\sigma}^2_{1,m},\end{aligned} \tag{56}$$

where the last line follows from Eq. (15) and the recognition that the second term of the second line is non-negative. □

Theorem 3. *Let $y(\mathbf{X})$ be a real-valued, square-integrable function with $\tilde{y}_{1,m}(\mathbf{X})$, $\hat{y}_{1,m}(\mathbf{X})$, and $\overline{y}_{1,m}(\mathbf{X})$ denoting its univariate additive PDD, univariate factorized PDD, and univariate hybrid PDD approximations, respectively, with $\tilde{\sigma}^2_{1,m}$, $\hat{\sigma}^2_{1,m}$, and $\overline{\sigma}^2_{1,m}$ as the variances obtained from respective approximations. If*

$$\tilde{e}_{1,m} := \mathbb{E}[y(\mathbf{X}) - \tilde{y}_{1,m}(\mathbf{X})]^2 = \mathbb{E}[w(\mathbf{X}) - \tilde{w}_{1,m}(\mathbf{X})]^2, \tag{57}$$

$$\hat{e}_{1,m} := \mathbb{E}[y(\mathbf{X}) - \hat{y}_{1,m}(\mathbf{X})]^2 = \mathbb{E}[w(\mathbf{X}) - \hat{w}_{1,m}(\mathbf{X})]^2, \tag{58}$$

and

$$\overline{e}_{1,m} := \mathbb{E}[y(\mathbf{X}) - \overline{y}_{1,m}(\mathbf{X})]^2 = \mathbb{E}[w(\mathbf{X}) - \overline{w}_{1,m}(\mathbf{X})]^2 \tag{59}$$

are the mean-squared errors committed by univariate additive PDD, univariate factorized PDD, and univariate hybrid PDD, respectively, in calculating σ^2, the variance of $y(\mathbf{X})$, then,

$$\overline{e}_{1,m} \le \tilde{e}_{1,m}$$

and

$$\overline{e}_{1,m} \le \hat{e}_{1,m}.$$

Proof. From Eqs. (57) and (59),

$$\tilde{e}_{1,m} = \sigma^2 - \tilde{\sigma}^2_{1,m} \tag{60}$$

and

$$\begin{aligned}\overline{e}_{1,m,m} &= \mathbb{E}[w^2(\mathbf{X})] + \mathbb{E}[\overline{w}^2(\mathbf{X})] - 2\mathbb{E}[w(\mathbf{X})\overline{w}_{1,m}(\mathbf{X})] \\ &= \sigma^2 + \overline{\sigma}^2_{1,m} - 2\mathbb{E}[w(\mathbf{X})\overline{w}_{1,m}(\mathbf{X})].\end{aligned} \tag{61}$$

Subtracting Eq. (60) from Eq. (61) yields

$$\begin{aligned}\overline{e}_{1,m} - \tilde{e}_{1,m} &= \overline{\sigma}^2_{1,m} - 2\mathbb{E}[w(\mathbf{X})\overline{w}_{1,m}(\mathbf{X})] + \tilde{\sigma}^2_{1,m} \\ &= (2\alpha_{1,m} - \alpha^2_{1,m})\tilde{\sigma}^2_{1,m} + (1-\alpha_{1,m})^2\hat{\sigma}^2_{1,m} + \tilde{\sigma}^2_{1,m} \\ &\quad - 2\mathbb{E}[w(\mathbf{X})\{\alpha_{1,m}\tilde{w}_{1,m}(\mathbf{X}) + (1-\alpha_{1,m})\hat{w}_{1,m}(\mathbf{X})\}] \\ &= 2(1-\alpha_{1,m})(\tilde{\sigma}^2_{1,m} - \mathbb{E}[w(\mathbf{X})\hat{w}_{1,m}(\mathbf{X})]) \\ &\quad + (1-\alpha_{1,m})^2(\hat{\sigma}^2_{1,m} - \tilde{\sigma}^2_{1,m}) \\ &= -(1-\alpha_{1,m})^2(\hat{\sigma}^2_{1,m} - \tilde{\sigma}^2_{1,m}) \le 0,\end{aligned} \tag{62}$$

following Lemma 1, where the second equality uses Eqs. (53) and (52) and the last equality uses Eq. (47).

Similarly, from Eq. (58),

$$\hat{e}_{1,m} = \sigma^2 + \hat{\sigma}^2_{1,m} - 2\mathbb{E}[w(\mathbf{X})\hat{w}_{1,m}(\mathbf{X})]. \tag{63}$$

Subtracting Eq. (63) from Eq. (61) yields

$$\begin{aligned}\overline{e}_{1,m} - \hat{e}_{1,m} &= \overline{\sigma}^2_{1,m} - 2\mathbb{E}[w(\mathbf{X})\overline{w}_{1,m}(\mathbf{X})] - \hat{\sigma}^2_{1,m} \\ &\quad + 2\mathbb{E}[w(\mathbf{X})\hat{w}_{1,m}(\mathbf{X})] \\ &= (2\alpha_{1,m} - \alpha^2_{1,m})\tilde{\sigma}^2_{1,m} + (1-\alpha_{1,m})^2\hat{\sigma}^2_{1,m} \\ &\quad - 2\mathbb{E}[w(\mathbf{X})\{\alpha_{1,m}\tilde{w}_{1,m}(\mathbf{X}) + (1-\alpha_{1,m})\hat{w}_{1,m}(\mathbf{X})\}] \\ &\quad - \hat{\sigma}^2_{1,m} + 2\mathbb{E}[w(\mathbf{X})\hat{w}_{1,m}(\mathbf{X})] \\ &= \tilde{\sigma}^2_{1,m} - \hat{\sigma}^2_{1,m} - 2\alpha_{1,m}(\tilde{\sigma}^2_{1,m} - \mathbb{E}[w(\mathbf{X})\hat{w}_{1,m}(\mathbf{X})]) \\ &\quad + (1-\alpha_{1,m})^2(\hat{\sigma}^2_{1,m} - \tilde{\sigma}^2_{1,m}) \\ &= -\alpha^2_{1,m}(\hat{\sigma}^2_{1,m} - \tilde{\sigma}^2_{1,m}) \le 0,\end{aligned} \tag{64}$$

following Lemma 1, where, again, the second equality uses Eqs. (53) and (52) and the last equality uses Eq. (47). □

The significance of Theorem 3 lies in providing analytical relations comparing the errors committed in calculating the variances by the univariate additive PDD, factorized PDD, and hybrid PDD approximations. It is clear from Theorem 3 that the error committed by univariate hybrid PDD can never be greater than the error committed by either univariate additive PDD or univariate factorized PDD.

5. Expansion coefficients

The determination of the expansion coefficients, $y_{\varnothing}$ and $C_{u\mathbf{j}_{|u|}}$ in Eqs. (2) and (8), respectively, involves various N-dimensional integrals over $\mathbb{R}^N$. For large N, a full numerical integration employing an N-dimensional tensor product of a univariate quadrature formula is computationally prohibitive. Instead, a dimension-reduction Gaussian-integration scheme and a sampling technique were applied to estimate the coefficients efficiently.

5.1. Dimension-reduction integration

The dimension-reduction integration, developed by Xu and Rahman [20], entails approximating a high-dimensional integral of interest by a finite sum of lower-dimensional integrations. For calculating the expansion coefficients $y_\varnothing$ and $C_{u\mathbf{j}_{|u|}}$, this is accomplished by replacing the N-variate function y in Eqs. (2) and (8) with an R-variate RDD approximation at a chosen reference point, where $R \le N$ [10,21]. The result is a reduced integration scheme, requiring evaluations of at most R-dimensional integrals.

Let $\mathbf{c} = (c_1, \ldots, c_N) \in \mathbb{R}^N$ be a reference point of $\mathbf{X}$ and $y(\mathbf{x}_v, \mathbf{c}_{-v})$ represent a $|v|-$variate component function of $y(\mathbf{x})$, $v \subseteq \{1, \ldots, N\}$. Replacing $y(\mathbf{x})$ with an R-variate truncation of its referential dimensional decomposition [10,21], the coefficients $y_\varnothing$ and $C_{u\mathbf{j}_{|u|}}$ are estimated from [20]

$$y_\varnothing \cong \sum_{k=0}^{R} (-1)^k \binom{N-R+k-1}{k} \sum_{\substack{v \subseteq \{1,\ldots,N\} \\ |v| = R-k}} \int_{\mathbb{R}^{|v|}} y(\mathbf{x}_v, \mathbf{c}_{-v}) f_{\mathbf{X}_v}(\mathbf{x}_v)\, d\mathbf{x}_v \tag{65}$$

and

$$C_{u\mathbf{j}_{|u|}} \cong \sum_{k=0}^{R} (-1)^k \binom{N-R+k-1}{k} \times \sum_{\substack{v \subseteq \{1,\ldots,N\} \\ |v| = R-k, u \subseteq v}} \int_{\mathbb{R}^{|v|}} y(\mathbf{x}_v, \mathbf{c}_{-v}) \psi_{u\mathbf{j}_{|u|}}(\mathbf{x}_u) f_{\mathbf{X}_v}(\mathbf{x}_v)\, d\mathbf{x}_v, \tag{66}$$

respectively, requiring evaluation of at most R-dimensional integrals. The reduced integration facilitates calculation of the coefficients approaching their exact values as $R \to N$, and is significantly more efficient than performing one N-dimensional integration, particularly when $R \ll N$. Hence, the computational effort is significantly decreased using the dimension-reduction integration. For instance, when $R=1$ or 2, Eqs. (65) and (66) involve one-, or at most, two-dimensional integrations, respectively.

For a general function y, numerical integrations are still required for performing various $|v|$-dimensional integrals over $\mathbb{R}^{|v|}$, $0 \le |v| \le R$, in Eqs. (65) and (66). When $R > 1$, multivariate numerical integrations are conducted by constructing a tensor product of underlying univariate quadrature rules. For a given $v \subseteq \{1, \ldots, N\}$, $1 < |v| \le R$, let $v = \{i_1, \ldots i_{|v|}\}$, where $1 \le i_1 < \cdots < i_{|v|} \le N$. Denote by $\{x_{i_p}^{(1)}, \ldots, x_{i_p}^{(n)}\} \subset \mathbb{R}$ a set of integration points of x_{i_p} and by $\{w_{i_p}^{(1)}, \ldots, w_{i_p}^{(n)}\}$ the associated weights generated from a chosen univariate quadrature rule and a positive integer $n \in \mathbb{N}$. Denote by $P^{(n)} = \times_{p=1}^{p=|v|} \{x_{i_p}^{(1)}, \ldots, x_{i_p}^{(n)}\}$ a rectangular grid consisting of all integration points generated by the variables indexed by the elements of v. Then the coefficients using dimension-reduction integration and numerical quadrature are approximated by

$$y_\varnothing \cong \sum_{i=0}^{R} (-1)^i \binom{N-R+i-1}{i} \sum_{\substack{v \subseteq \{1,\ldots,N\} \\ |v| = R-i}} \sum_{\mathbf{k}_{|v|} \in P^{(n)}} w^{(\mathbf{k}_{|v|})} y(\mathbf{x}_v^{(\mathbf{k}_{|v|})}, \mathbf{c}_{-v}) \tag{67}$$

and

$$C_{u\mathbf{j}_{|u|}} \cong \sum_{i=0}^{R} (-1)^i \binom{N-R+i-1}{i} \times \sum_{\substack{v \subseteq \{1,\ldots,N\} \\ |v| = R-i, u \subseteq v}} \sum_{\mathbf{k}_{|v|} \in P^{(n)}} w^{(\mathbf{k}_{|v|})} y(\mathbf{x}_v^{(\mathbf{k}_{|v|})}, \mathbf{c}_{-v}) \psi_{u\mathbf{j}_{|u|}}(\mathbf{x}_u^{(\mathbf{k}_{|u|})}), \tag{68}$$

where $\mathbf{x}_v^{(\mathbf{k}_{|v|})} = \{x_{i_1}^{(k_1)}, \ldots, x_{i_{|v|}}^{(k_{|v|})}\}$ and $w^{(\mathbf{k}_{|v|})} = \prod_{p=1}^{p=|v|} w_{i_p}^{(k_p)}$ is the product of integration weights generated by the variables indexed by the elements of v. For independent coordinates of $\mathbf{X}$, as assumed here, a univariate Gauss quadrature rule is commonly used, where the integration points and associated weights depend on the probability distribution of X_i. They are readily available, for example, the Gauss–Hermite or the Gauss–Legendre quadrature rule, when X_i follows Gaussian or uniform distribution. An n-point Gauss quadrature rule exactly integrates a polynomial with a total degree of at most $2n-1$.

The S-variate, mth-order PDD approximation requires evaluations of $\sum_{k=0}^{k=S} \binom{N}{k} m^k$ expansion coefficients, including $y_\varnothing(\mathbf{d})$. If these coefficients are estimated by dimension-reduction integration with $R = S < N$ and, therefore, involve at most an S-dimensional tensor product of an n-point univariate quadrature rule depending on m, then the total cost for the S-variate, mth-order approximation entails a maximum of $\sum_{k=0}^{k=S} \binom{N}{k} n^k(m)$ function evaluations. If the integration points include a common point in each coordinate – a special case of symmetric input probability density functions and odd values of n – the number of function evaluations reduces to $\sum_{k=0}^{k=S} \binom{N}{k} (n(m)-1)^k$. Nonetheless, the computational complexity of the S-variate PDD approximation is an Sth-order polynomial with respect to the number of random variables or integration points. Therefore, PDD with dimension-reduction integration of the expansion coefficients alleviates the curse of dimensionality to an extent determined by S.

5.2. Quasi-Monte Carlo simulation

Employing the quasi-MCS method for the estimation of the PDD expansion coefficients, which are high-dimensional integrals defined in Eqs. (2) and (8), again comprises three simple steps: (1) generate a low-discrepancy point set $\mathcal{P}_L := \{\mathbf{u}^{(k)} \in [0,1]^N, k = 1, \ldots, L\}$ of size $L \in \mathbb{N}$; (2) map each sample from $\mathcal{P}_L$ to the sample $\mathbf{x}^{(k)} \in \mathbb{R}^N$ following the probability measure of the random input $\mathbf{X}$; and (3) approximate the coefficients by

$$y_\varnothing \cong \frac{1}{L} \sum_{k=1}^{L} y(\mathbf{x}^{(k)}), \tag{69}$$

$$C_{u\mathbf{j}_{|u|}} \cong \frac{1}{L} \sum_{k=1}^{L} y(\mathbf{x}^{(k)}) \psi_{u\mathbf{j}_{|u|}}(\mathbf{x}_u^{(k)}). \tag{70}$$

6. Numerical examples

Two numerical examples are presented to illustrate the hybrid PDD method developed in calculating the second-moment statistics and tail probability distributions of random mathematical functions and random eigensolutions of a simple stochastic dynamical system. Classical Legendre polynomials were used to define the orthonormal polynomials in Example 1, and all PDD expansion coefficients and the hybrid model parameter were determined analytically. In Example 2 all original random variables were transformed into standard Gaussian random variables, facilitating the use of classical Hermite orthonormal polynomials as bases. The expansion coefficients in Example 2 were calculated using dimension-reduction integration ($R=1$) involving the five-point univariate Gauss–Hermite quadrature rule. The hybrid model parameter was estimated by quasi-MCS using Sobol's low-discrepancy sequence of 100 and 500 points and Eq. (54). The sample size for the embedded MCS in Example 2 is 10^6.

6.1. Polynomial function

Consider the polynomial function

$$y(\mathbf{X}) = \left[\frac{2}{N} \sum_{i=1}^{N} X_i\right]^q,$$

where $N=5$, X_i, $i=1,\ldots,N$, are independent and identical random variables, each following the standard uniform distribution over $[0,1]$, and $q \in \mathbb{N}$ is an exponent. The function $y(\mathbf{X})$ has a purely additive structure when $q=1$, but as the value of q increases, the

function $y(\mathbf{X})$ evolves from strongly additive to strongly multiplicative. The objective of this example is to compare univariate additive PDD, univariate factorized PDD, and univariate hybrid PDD approximations in calculating the variance of $y(\mathbf{X})$ for $q=2, 3, 4, 5, 6, 7, 8$.

Since y is a multivariate polynomial of degree q, the truncation parameter m for a PDD approximation, whether additive, factorized, or hybrid, was set equal to q. Fig. 1 shows how the hybrid model parameter $\alpha_{1,m}$ varies with respect to q, where $\tilde{\sigma}^2_{1,m}$, $\hat{\sigma}^2_{1,m}$, and the expectation in Eq. (46) of $\alpha_{1,m}$ are calculated exactly. The parameter $\alpha_{1,m}$ is relatively close to one when $q=2$, and decreases monotonically as q increases, indicating the diminishing additive structure of the function y. When $q=8$, $\alpha_{1,m}$ is relatively close to zero, that is, y is dominantly multiplicative.

Fig. 2 presents the relative errors, defined as the ratio of the absolute difference between the exact and approximate variances of $y(\mathbf{X})$ to the exact variance, committed by the univariate additive PDD, univariate factorized PDD, and univariate hybrid PDD methods. The second-moment properties of $y(\mathbf{X})$, given q, were calculated exactly. The function $y(\mathbf{X})$ is strongly additive when $q=2$ or 3; therefore, the univariate additive PDD approximation has lower error than the factorized PDD approximation. But the trend reverses for $4 \le q \le 8$, the range of higher values examined. This is because the function switches from dominantly additive ($q \le 3$) to dominantly multiplicative ($q > 3$) as q increases. Nonetheless, for all the values of q considered, the univariate hybrid PDD approximation commits lower errors than either univariate additive PDD or univariate factorized PDD approximation. These results are consistent with the findings of Theorem 3.

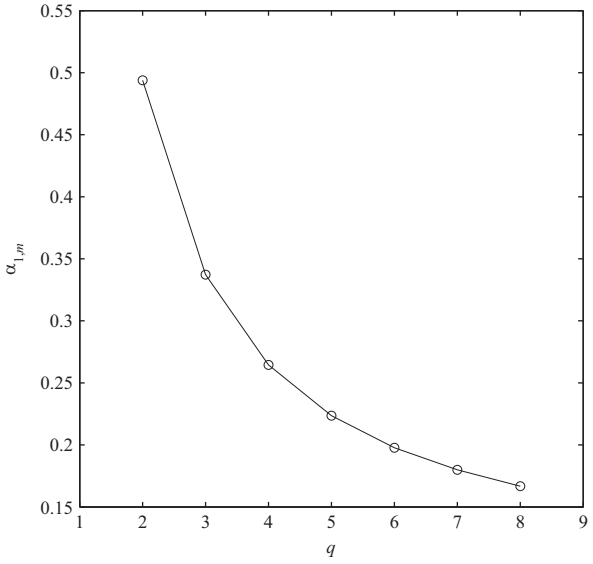

Fig. 1. Variation of $\alpha_{1,m}$ with respect to q (Example 1).

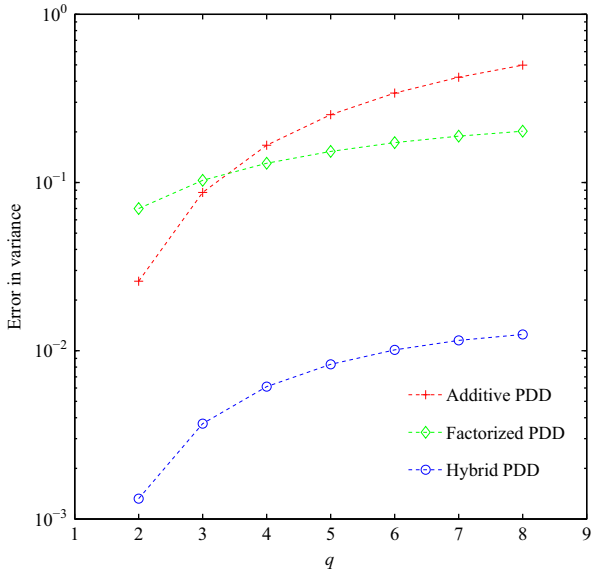

Fig. 2. Error in variance calculation from additive PDD, factorized PDD, and hybrid PDD approximations (Example 1).

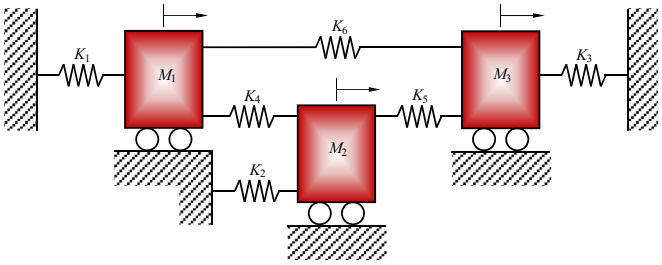

Fig. 3. A three-degree-of-freedom, undamped, spring–mass system (Example 2).

6.2. Three-degree-of-freedom, undamped, spring–mass system

Consider a three-degree-of-freedom, undamped, spring–mass system, shown in Fig. 3, with random mass and random stiffness matrices

$$\mathbf{M}(\mathbf{X}) = \begin{bmatrix} M_1(\mathbf{X}) & 0 & 0 \\ 0 & M_2(\mathbf{X}) & 0 \\ 0 & 0 & M_3(\mathbf{X}) \end{bmatrix} \tag{71}$$

and

$$\mathbf{K}(\mathbf{X}) = \begin{bmatrix} K_{11}(\mathbf{X}) & K_{12}(\mathbf{X}) & K_{13}(\mathbf{X}) \\ & K_{22}(\mathbf{X}) & K_{23}(\mathbf{X}) \\ (\text{sym.}) & & K_{33}(\mathbf{X}) \end{bmatrix}, \tag{72}$$

respectively, where $K_{11}(\mathbf{X}) = K_1(\mathbf{X}) + K_4(\mathbf{X}) + K_6(\mathbf{X})$, $K_{12}(\mathbf{X}) = -K_4(\mathbf{X})$, $K_{13}(\mathbf{X}) = -K_6(\mathbf{X})$, $K_{22}(\mathbf{X}) = K_4(\mathbf{X}) + K_5(\mathbf{X}) + K_2(\mathbf{X})$, $K_{23}(\mathbf{X}) = -K_5(\mathbf{X})$, and $K_{33}(\mathbf{X}) = K_5(\mathbf{X}) + K_3(\mathbf{X}) + K_6(\mathbf{X})$; the masses $M_i(\mathbf{X}) = \mu_i X_i$; $i = 1, 2, 3$ with $\mu_i = 1.0$ kg; $i = 1, 2, 3$, and spring stiffnesses $K_i(\mathbf{X}) = \mu_{i+3} X_{i+3}$; $i = 1, \ldots, 6$ with $\mu_{i+3} = 1.0$ N/m; $i = 1, \ldots, 5$ and $\mu_9 = 3.0$ N/m. The input $\mathbf{X} = \{X_1, \ldots, X_9\}^T \in \mathbb{R}^9$ is an independent lognormal random vector with mean $\boldsymbol{\mu}_{\mathbf{X}} = \mathbf{1} \in \mathbb{R}^9$ and covariance matrix $\boldsymbol{\Sigma}_{\mathbf{X}} = \nu^2 \mathbf{I} \in \mathbb{R}^{9\times 9}$ with coefficient of variation $\nu = 0.3$.

The primary objective of this example is to demonstrate the high accuracy of univariate hybrid PDD approximation in calculating the cumulative distribution functions of the three eigenvalues of the three-degree-of-freedom system. The secondary, although significant, objective of this example is to show that the quasi-MCS method, with a relatively small sample size for calculating the model parameter of univariate hybrid PDD approximation, is capable of delivering results comparable to those obtained from the expensive bivariate additive PDD approximation.

The probability distributions of three eigenvalues of the three-degree-of-freedom system were calculated using the benchmark solution of 10^6 crude MCS method, and five different fourth-order ($m = 4$) PDD methods: (1) univariate additive PDD, (2) bivariate additive PDD, (3) univariate factorized PDD, (4) univariate hybrid PDD with $\alpha_{1,4}$ estimated using 100 quasi-MCS samples, and (5) univariate hybrid PDD with $\alpha_{1,4}$ estimated using 500 quasi-MCS samples. Fig. 4 presents the marginal probability distributions

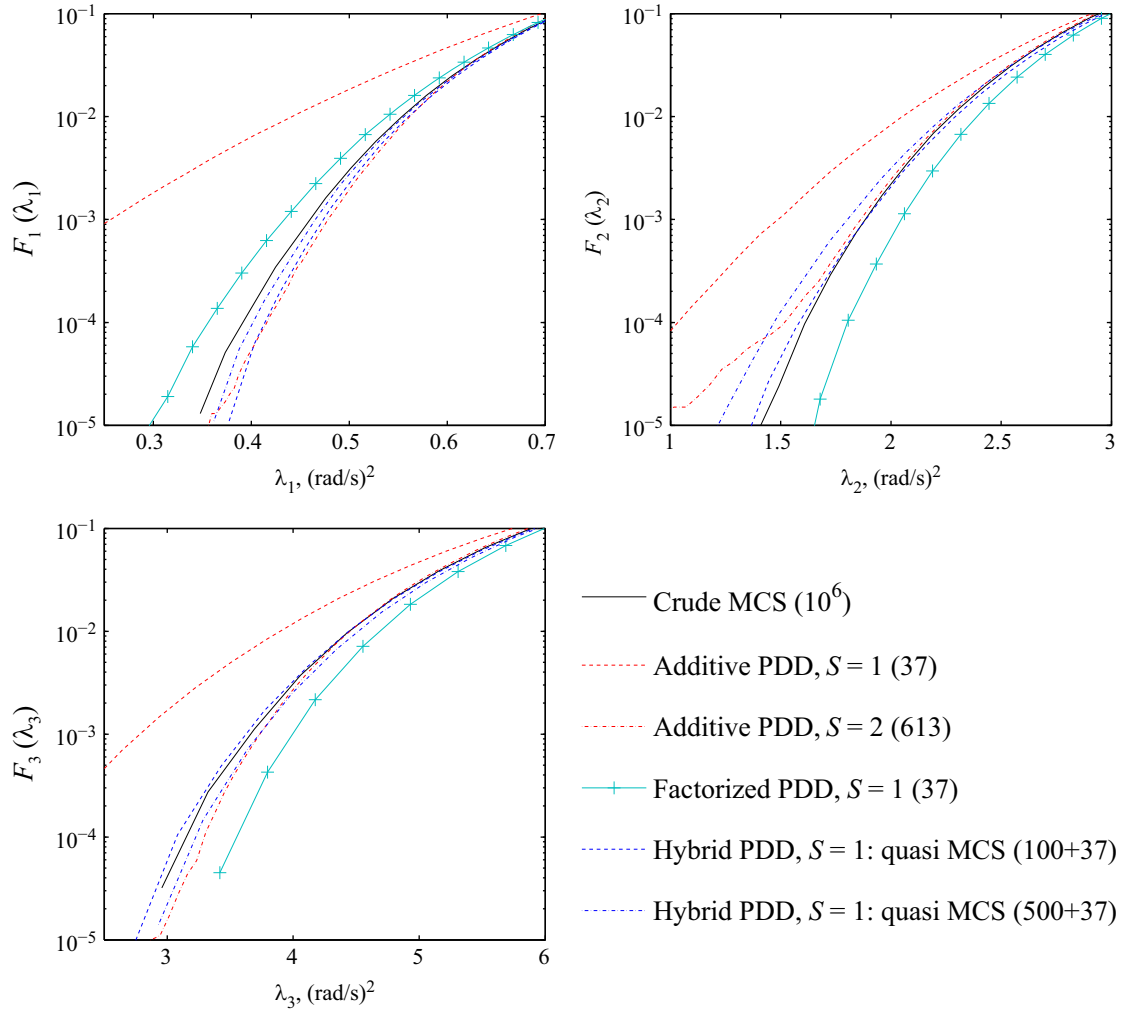

Fig. 4. Tail probabilities of three eigenvalues of the three-degree-of-freedom, undamped, spring–mass system by various PDD approximations and crude MCS.

$F_i(\lambda_i) := P[\Lambda_i \le \lambda_i]$ of three eigenvalues λ_i, $i = 1, 2, 3$, where all the PDD solutions were obtained from the embedded MCS; the parenthetical values reflect the total number of function evaluations required by the respective methods. The plots are made over a semi-logarithmic scale to delineate the distributions in the tail regions. For all three eigenvalues, the probability distributions obtained from the univariate additive PDD method are far from the crude MCS results, divulging the clear inadequacy of the univariate additive PDD approximation in calculating tail probabilities. The univariate factorized PDD method performs relatively better than its additive counterpart, indicating the dominantly multiplicative structure of the functions; however, it still leaves much room for improvement compared with the benchmark crude MCS results. The univariate hybrid PDD method requires additional computational effort owing to quasi-MCS for estimating $\alpha_{1,4}$ in Eq. (54), but the improved results obtained clearly justify the additional cost. To put the results of the univariate hybrid PDD method in perspective, the results from the bivariate ($S = 2$) additive PDD method, also obtained, show dramatic improvement over the univariate additive PDD method, as expected. However, the bivariate additive PDD method also leads to a significantly larger number of function evaluations compared with the univariate hybrid PDD with quasi-MCS (100 samples). Therefore, a hybrid PDD approximation is desirable, where only univariate truncations are feasible, but not necessarily rendering adequate accuracy in stochastic solutions by either additive or factorized PDD approximation alone.

7. Application: a pickup truck

This section illustrates the effectiveness of the proposed hybrid PDD method in solving a large-scale practical engineering problem. The application involves predicting the probabilistic characteristics of sound pressure levels inside the cabin of a pickup truck. The acoustics, measured through sound pressure levels, inside a vehicle are widely considered as a prominent parameter revealing the overall quality and build of the vehicle. A coupled acoustic-structural analysis is therefore critically important in the automotive industry as it paves the way towards designing vehicles for ride comfort and quietness. Fig. 5(a) presents a computer-aided design (CAD) cabin–air–chassis model of a pickup truck [22]. A finite-element analysis (FEA) mesh of the model, comprising 43,663 structural elements used to model the cabin and the chassis and 12,171 acoustic elements used to model the air interior, with a total of 207,994 degrees of freedom, is displayed in Fig. 5(b). Fig. 6(a) depicts the cabin model without air mesh and doors to show the space occupied by the air mesh, and Fig. 6(b) displays the air mesh that fills the cabin interior. A tie constraint was employed to connect the air mesh to the structural parts inside the cabin surface or onto the seat surface.

Portrayed in Fig. 5(a), the CAD model contains 24 distinct materials, with 22 structural materials and two non-structural materials representing the air inside the cabin and the carpet on the cabin floor. Twenty-one of the structural materials were modeled as shell elements, and the remaining material as beam

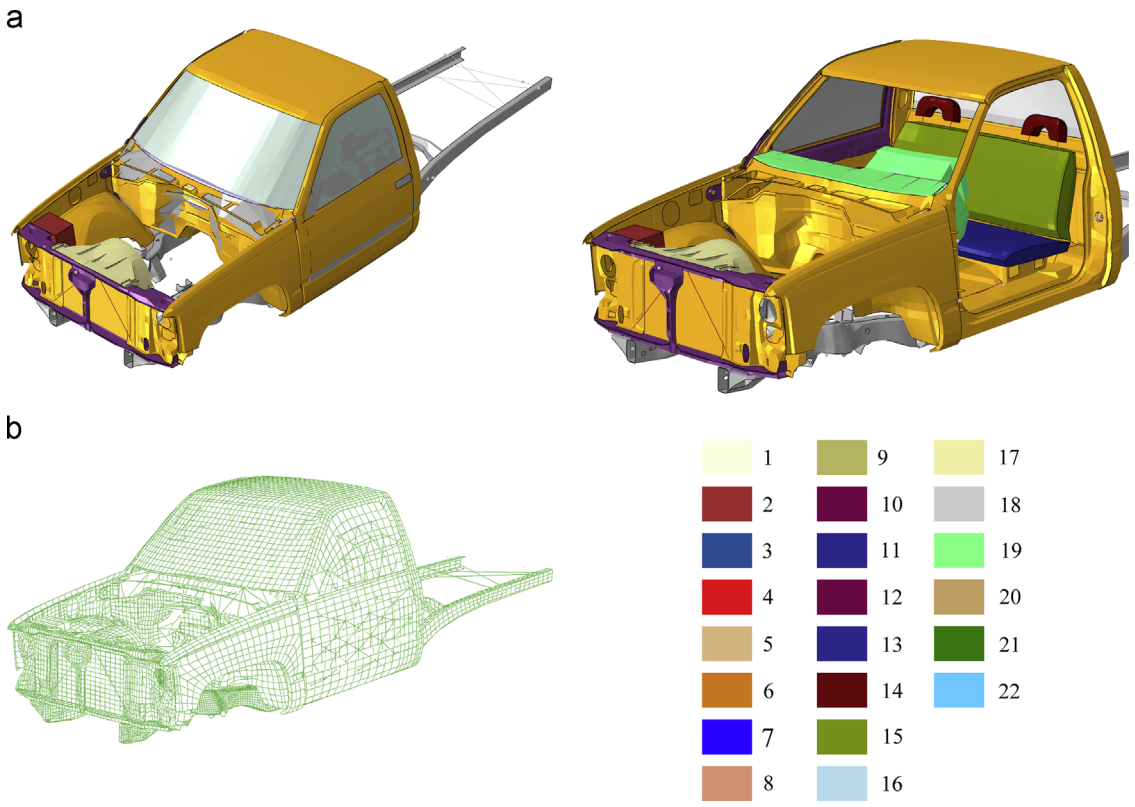

Fig. 5. Cabin–air–chassis model of pickup truck: (a) a CAD model, (b) an FEA mesh.

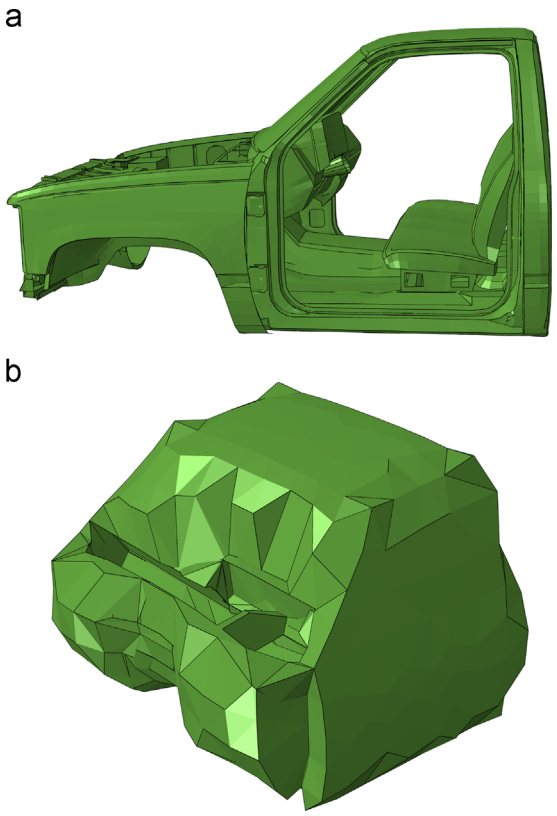

Fig. 6. Cabin of pickup truck and air mesh. (a) Cabin model of pickup truck with doors removed for clearer illustration; (b) the air mesh inside the cabin.

elements defining the circular beam used for headrest mounting. Young's moduli of 22 structural materials are random variables. The mass densities of the 21 materials modeled as shell elements are also random variables. Apart from the structural material properties, the bulk modulus and the mass density of the air inside the cabin are also random variables. Finally, the proportionality factor between the pressure and the velocity of the carpet surface in the normal direction is also a random variable. This proportionality constant defines the acoustic admittance of the carpet surface on the cabin floor. In aggregate, there exist 46 random variables $X_i = 1, \ldots, 46$, as follows: X_1 to X_{22}=Young's moduli of materials 1–22; X_{23} to X_{43}=mass densities of materials 1–21; X_{44}=bulk modulus of air inside the cabin; X_{45}=mass density of air inside the cabin; and X_{46}=acoustic admittance of the carpet surface on the cabin floor. All 46 random variables are independent and uniformly distributed with the coefficient of variation equal to 0.2. Table 1 presents the material and part names, and the means of random variables corresponding to the 22 structural materials, $\mu_i := \mathbb{E}[X_i]$, $i = 1, \ldots, 43$. The means of the bulk modulus and mass density of air inside the cabin are $\mu_{44} = 0.139$ GPa and $\mu_{45} = 1.2 \times 10^{-12}$ kg/mm^3. The mean of the acoustic admittance of the carpet surface on the cabin floor is $\mu_{46} = 0.5 \times 10^6$ mm^2 s/kg. All structural materials, except materials 8, 9, and 10, have a deterministic Rayleigh stiffness proportional damping defined by the parameter $\beta_R = 0.4 \times 10^{-6}$ s. For a given value of β_R, the damping fraction ξ_i for a mode i with natural frequency ω_i is given by the formula $\xi_i = \beta_R \omega_i / 2$. The value of β_R chosen in this model is to give approximately 1 percent critical damping for the modes whose natural frequencies are in the middle of the range of excitation, i.e., at about 80 Hz at mean input. Poisson's ratios of all structural materials are deterministic and are equal to 0.3. The probability distributions of input random variables in this problem were chosen arbitrarily, as the main purpose was to demonstrate the ability of the proposed method in solving large-scale practical engineering problems. Identifying more realistic probability distributions for each material will require additional studies that are beyond the scope of this work.

Table 1
Material, part name, and mean values of the random input variables for structural materials in pickup truck.

Material	Material name	Young's modulus (GPa)	Mass density (kg/m^3)	Part name
1	Steel	210	7890	Rail (chassis), bed, cabin, fenders, engine oil box
2	Steel	210	7890	Wheel housings, rear rim, steering support, battery tray, seat track
3	Steel	210	7890	Radiator mounting, radiator outer, fan center, fuel tank
4	Steel	210	7890	Engine mountings, fender mountings, hood, doors, cabin hinges
5	Plastic	2.8	1200	Fan cover
6	Glass	76	2500	Windows, windshield
7	Plastic	3.4	1100	Radiator side block
8	Steel	210	7890	Rear axle, drive shaft, steering, steering column, gearbox CV joint, brakes
9	Steel	210	20,900	Brake assembly
10	Steel	210	6910	Brake assembly
11	Rubber	250	8060	Tires
12	Steel	210	7890	A-arm mountings, A-arm–rim connectors, A-arm–rail connectors, front rim, bed–rail connector, rail connector
13	Foam	2.0	253	Seat bottom
14	Foam	2.0	755	Seat top
15	Foam	2.0	169	Seat headrest
16	Steel	210	2500	Door lock
17	Steel	200	7800	Radiator
18	Rubber–metal composite	210	1960	Battery
19	Steel	120	3890	Engine gearbox
20	Steel	21	1820	Engine front
21	Steel	210	7890	Headrest connector beams, fan, door lock beams, oil pan beams, dashboard support
22	Steel	210	–[a]	Radiator mounting beams

[a] Not required.

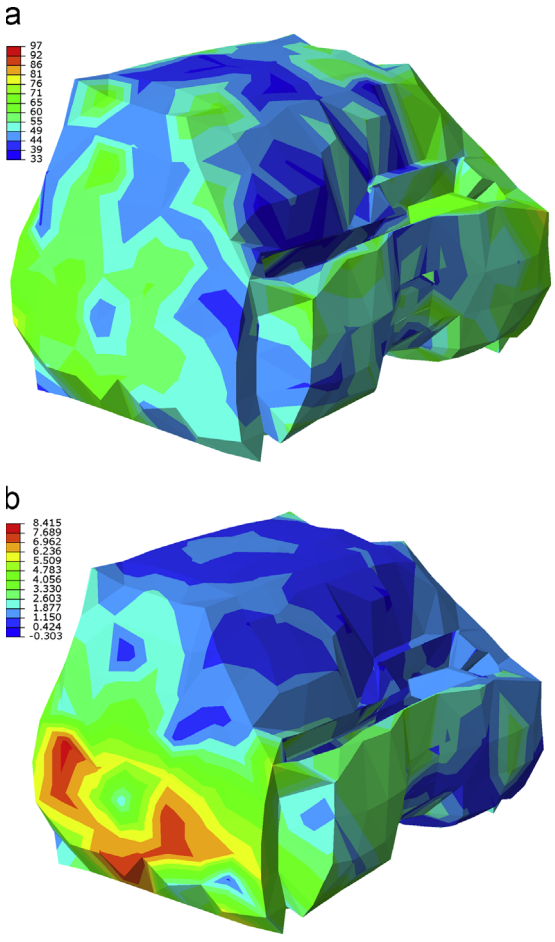

Fig. 7. Contour plots of the $\mathcal{L}_2$-norms of 35th mode shape of air inside the cabin of a pickup truck by the hybrid PDD approximation: (a) mean, (b) variance.

7.1. Coupled acoustic-structural analysis

A mode-based coupled acoustic-structural analysis consists of two steps: an eigensolution extraction followed by a steady-state dynamic analysis involving sound pressure level calculations. For obtaining eigensolutions, the first 200 eigenfrequencies were extracted. The Lanczos method [23] embedded in Abaqus (Version 6.12) [22] was employed for extracting natural frequencies and mode shapes. For steady-state dynamic analysis, the airborne load originating from engine vibration was modeled as a diffuse field incident wave loading on the bulkhead below the dashboard. In the steady-state dynamic analysis, the sound pressure level at a location in the vicinity of the driver's ear was calculated. The location of the driver's ear was defined through a node in the air mesh inside the cabin, in accordance with the specifications of location for measurement of noise inside motor vehicles defined in International Standard ISO-5128 [24]. The values of the sound pressure level were calculated at 200 evenly spaced points in the excitation frequency range of 35–120 Hz. This frequency range corresponds to engine-induced vibrations in the range of 2100–7200 rpm. The governing equations of a coupled acoustic-structural analysis are described in Appendix A.

Due to the uncertainty in material properties, the eigensolutions and sound pressure level values are random functions. The univariate, second-order hybrid PDD approximation was employed to determine their second-moment characteristics and various response probabilities. The associated expansion coefficients of PDD and the hybrid model parameter were estimated by the quasi-MCS method with 500 samples. The sample size for the embedded MCS of the PDD approximation is 5000.

7.2. Moments of mode shapes

The univariate, second-order hybrid PDD method was employed to calculate the second-moment statistics of each nodal pressure component of an eigenvector describing the associated

mode shape of the air inside the cabin. All input random variables were transformed into uniform random variables, permitting the use of Legendre orthonormal polynomials as basis functions. The second-moment statistics were calculated from Eqs. (69) and (53) where the hybrid model parameter was estimated from Eq. (55). Based on these statistics, the $\mathcal{L}_2$-norms (square root of sum of squares) of the mean and variance of a nodal pressure were calculated. Fig 7(a) and (b) presents contour plots of the $\mathcal{L}_2$-norms of the mean and variances, respectively, of an arbitrarily selected 35th mode shape, calculated using hybrid PDD approximation. Similar results can be generated for other mode shapes if desired.

7.3. Probabilistic characteristics of sound pressure level

The sound pressure level in decibels (dB) is calculated in the vicinity of the driver's ear as $\mathrm{SPL} = 20\log_{10}[p/(p_{ref}\sqrt{2})]$, where p is the pressure in Pa obtained in mode-based steady-dynamic analysis, and $p_{ref} = 2\times10^{-5}$ Pa is the *zero* or reference sound pressure, which is considered as the threshold of human hearing. Fig. 8 shows various percentiles of sound pressure level in the vicinity of the driver's ear calculated from the univariate, second-order hybrid PDD approximation. The percentiles were calculated from 5000 embedded MCS of the hybrid PDD approximation at 200 evenly spaced points in the excitation frequency range of 35–120 Hz. Fig. 9 presents the probability density function of the maximum sound pressure level in the excitation frequency range of 35–120 Hz, as calculated from 5000 embedded MCS of the hybrid PDD approximation. These results provide vital information pertaining to the acoustic performance of the vehicle operating under several random input parameters. A designer can utilize these valuable results for optimizing the vehicle design to achieve a desired acoustic performance.

8. Conclusion

A new hybrid PDD method was developed for uncertainty quantification of high-dimensional complex systems. The method is built from a linear combination of an additive and a multiplicative PDD approximation, both obtained from lower-dimensional ANOVA component functions of a general, square-integrable multivariate function. When a stochastic response is not endowed with a specific dimensional hierarchy, the hybrid PDD approximation, optimally blending the additive PDD and multiplicative PDD approximations, is the best choice. A theorem and a corollary proven herein give analytical expressions for the model parameters that form the linear combinations of additive PDD and multiplicative PDD approximations, resulting in the hybrid PDD method. Using properties of orthonormal polynomials, explicit formulae were derived for calculating the response statistics by the univariate hybrid PDD approximation.

The univariate truncation of the hybrid PDD was employed to calculate the second-moment properties and tail probability distribution in two numerical problems, where the output functions are either simple mathematical functions or eigenvalues of a simple linear oscillator. For a function with a mixed additive and multiplicative structure, the univariate hybrid PDD approximation commits remarkably lower errors in calculating the variance compared with both univariate additive and multiplicative PDD approximations. The univariate hybrid PDD approximation is also more accurate than either the univariate additive or multiplicative PDD methods, and is more efficient than the bivariate additive PDD method in determining the tail probabilistic characteristics of eigenvalues of the dynamic system examined. Therefore, the univariate truncation of the hybrid PDD is ideally suited to solving stochastic problems that may otherwise mandate expensive bivariate or higher-variate additive or multiplicative PDD approximations. Finally, a successful evaluation of random eigensolutions of a pickup truck, subjected to 46 input random variables, involving coupled acoustic-structure analysis demonstrates the ability of the new method in solving large-scale practical engineering problems.

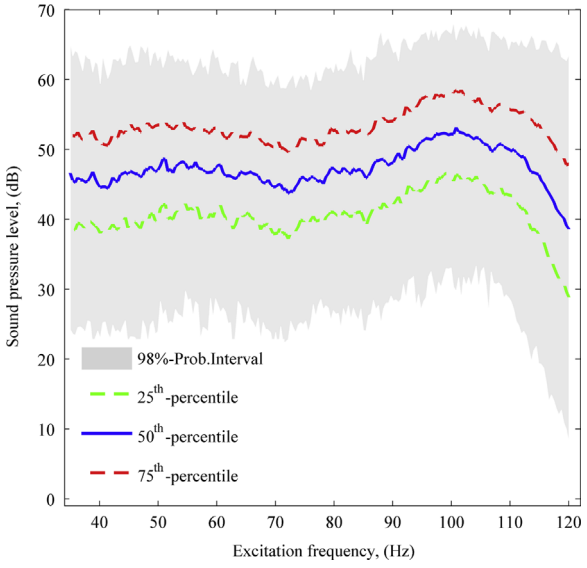

Fig. 8. Percentiles of sound pressure levels in the vicinity of the driver's ear in a pickup truck by the hybrid PDD approximation.

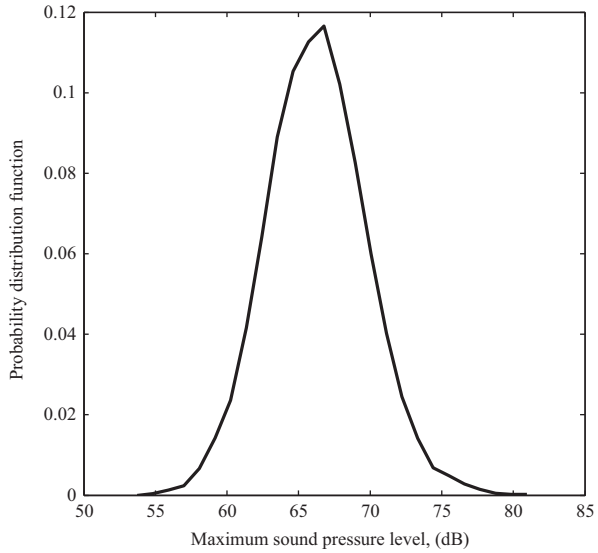

Fig. 9. Probability density function of the maximum sound pressure level in excitation frequency range of 35–120 Hz by the hybrid PDD approximation.

Appendix A. Governing equations for coupled acoustic-structural analysis

A coupled acoustic-structural analysis involves solution of the acoustic variational equation

$$\int_{V_f}\left[\delta p\left(\frac{1}{K_f}\ddot{p}+\frac{\gamma}{\rho_f K_f}\dot{p}\right)+\frac{1}{\rho_f}\frac{\partial\delta p}{\partial\mathbf{x}}\cdot\frac{\partial p}{\partial\mathbf{x}}\right]dV-\int_{S_{fi}}\delta p T_0\,dS$$
$$+\int_{S_{fr}}\delta p\left(\frac{\gamma}{\rho_f c_1}p+\left(\frac{\gamma}{\rho_f k_1}+\frac{1}{c_1}\right)\dot{p}+\frac{1}{k_1}\ddot{p}\right)dS$$

$$+\int_{S_{fi}}\delta p\left(\frac{1}{c_1}\dot{p}+\frac{1}{a_1}p\right)dS-\int_{S_{fs}}\delta p\mathbf{n}^-\cdot\ddot{\mathbf{u}}^m\,dS$$
$$+\int_{S_{frs}}\delta p\left(\frac{\gamma}{\rho_f c_1}p+\left(\frac{\gamma}{\rho_f k_1}+\frac{1}{c_1}\right)\dot{p}+\frac{1}{k_1}\ddot{p}-\mathbf{n}^-\cdot\ddot{\mathbf{u}}^m\right)dS=0, \quad (A.1)$$

and the structural virtual work equation

$$\int_V\delta\epsilon:\sigma\,dV+\int_V\alpha_c\rho\delta\mathbf{u}^m\cdot\dot{\mathbf{u}}^m\,dV+\int_V\rho\delta\mathbf{u}^m\cdot\ddot{\mathbf{u}}^m\,dV$$
$$+\int_{S_{fs}}p\delta\mathbf{u}^m\cdot\mathbf{n}\,dS-\int_{S_t}\delta\mathbf{u}^m\cdot\mathbf{t}\,dS=0 \quad (A.2)$$

simultaneously for the structural displacement $\mathbf{u}^m$ and the acoustic "displacement" or pressure p. In Eqs. (A.1) and (A.2), K_f is the bulk modulus of the fluid acoustic medium of volume V_f; γ is the volumetric drag, or force per unit volume per velocity, in the fluid; ρ_f is the mass density of the fluid; δp is the pressure variation in the fluid; $\mathbf{x}$ is spatial position of the fluid particle; T_0 is the prescribed boundary traction over S_{ft}, the acoustic boundary subregion where the normal derivative of the acoustic medium is prescribed; $1/c_1$ and $1/k_1$ are the proportionality coefficients between the pressure and velocity, and the pressure and displacement, respectively, normal to the surface of the fluid; S_{fr} is the reactive acoustic boundary subregion; S_{fi} is the radiating acoustic boundary subregion; S_{frs} is the acoustic boundary subregions where the displacements are linearly coupled but not necessarily identically equal due to the presence of a compliant or reactive intervening layer; $\mathbf{n}^-$ is the outward normal to the structure; σ is the stress at a point on the structure; $\delta\epsilon$ is the strain variation in the structure; α_c is the mass proportional damping factor; ρ is the mass density of the structure; and $\mathbf{t}$ is the surface traction applied over the surface S_t of the structure. Further details are available elsewhere [25].

References

[1] Rahman S. A polynomial dimensional decomposition for stochastic computing. Int J Numer Methods Eng 2008;76:2091–2116.
[2] Rahman S. Extended polynomial dimensional decomposition for arbitrary probability distributions. J Eng Mech 2009;135:1439–1451.
[3] Rahman S, Yadav V. Orthogonal polynomial expansions for solving random eigenvalue problems. Int J Uncertain Quantif 2011;1:163–187.
[4] Yadav V, Rahman S. Adaptive-sparse polynomial dimensional decomposition methods for high-dimensional stochastic computing. Comput Methods Appl Mech Eng 2014;274:56–83.
[5] Bellman R. Dynamic programming. Princeton, NJ: Princeton University Press; 1957.
[6] Morokoff WJ, Caflisch RE. Quasi-Monte Carlo integration. J Comput Phys 1995;122:218–230.
[7] Yadav V, Rahman S. Uncertainty quantification of high-dimensional complex systems by multiplicative polynomial dimensional decompositions. Int J Numer Methods Eng 2013;94:221–247.
[8] Sobol IM. Theorems and examples on high dimensional model representation. Reliab Eng Syst Saf 2003;79:187–193.
[9] Kuo FY, Sloan IH, Wasilkowski GW, Wozniakowski H. On decompositions of multivariate functions. Math Comput 2011;79:953–966.
[10] Rahman S. Approximation errors in truncated dimensional decompositions. Math Comput 2014;83:2799–2819.
[11] Rahman S. Statistical moments of polynomial dimensional decomposition. J Eng Mech 2010;136:923–927.
[12] Tunga MA, Demiralp M. A factorized high dimensional model representation on the nodes of a finite hyperprismatic regular grid. Appl Math Comput 2005;164:865–883.
[13] Rahman S. Uncertainty quantification by alternative decompositions of multivariate functions. SIAM J Sci Comput 2013;35:A3024–A3051.
[14] Niederreiter H. Random number generation and quasi-Monte Carlo methods, CBMS-NSF regional conference series in applied mathematics. Society for Industrial and Applied Mathematics, Philadelphia, PA, USA; 1992.
[15] Halton J. On the efficiency of certain quasi-random sequences of points in evaluating multi-dimensional integrals. Numer Math 1960;2:84–90.
[16] Faure H. Discrépances de suites associées à un système de numération (en dimension un). Bull Soc Math France 1981;109:143–182.
[17] Sobol IM. On the distribution of points in a cube and the approximate evaluation of integrals. USSR Comput Math Math Phys 1967;7:86–112.
[18] Sloan I, Joe S. Lattice methods for multiple integration. Oxford Science Publications, Clarendon Press, Oxford, UK; 1994.
[19] Wang X. Improving the rejection sampling method in quasi-Monte Carlo methods. J Comput Appl Math 2000;114:231–246.
[20] Xu H, Rahman S. A generalized dimension-reduction method for multidimensional integration in stochastic mechanics. Int J Numer Methods Eng 2004;61:1992–2019.
[21] Xu H, Rahman S. Decomposition methods for structural reliability analysis. Probab Eng Mech 2005;20:239–250.
[22] ABAQUS Standard, Version 6.12, Dassault Systems Simulia Corp, 2012.
[23] Cullum JK, Willoughby RA. Lanczos algorithms for large symmetric eigenvalue computations: theory, classics in applied mathematics. Society for Industrial and Applied Mathematics, Philadelphia, PA, USA; 2002.
[24] ISO-5128, Acoustics—measurement of noise inside motor vehicles, International Organization for Standardization, Geneva, Switzerland; 1980.
[25] Morse P, Ingard K. Theoretical acoustics. McGraw-Hill, Princeton University Press, Princeton, NJ, USA; 1968.